Title: Network-based modelling reveals cell-type enriched patterns of non-coding RNA regulation during human skeletal muscle remodelling

Authors: Jonathan C. Mcleod [1], Changhyun Lim[1,2], Tanner Stokes[1], Jalil-Ahmad Sharif [3], Vagif Zeynalli [1], Lucas Wiens [1], Alysha C D'Souza [1], Lauren Colenso-Semple [1], James McKendry [1,4], Robert W. Morton [1], Cameron J. Mitchell [5], Sara Y. Oikawa [1], Claes Wahlestedt [6], J Paul Chapple [3], Chris McGlory [7], James A. Timmons [3,6*] and Stuart M. Phillips [1*]

Short-title: RNA profiling of ncRNA genes in skeletal muscle

One Sentence Summary: We used an optimised transcriptomic strategy to identify a set of ncRNA genes regulated during skeletal muscle hypertrophy in one hundred and forty-four people, with network modelling and spatial imaging providing biological context.

Key words: Transcriptome, Angiogenesis, Spatial, Muscle Growth, Exercise, Single-Cell, Immune Cell

Affiliations:

[1]Department of Kinesiology, McMaster University, Hamilton, Ontario, Canada.

[2] Population Health Sciences Institute, Faculty of Medicial Sciences, Newcastle University, Newcastle upon Tyne, UK

[3] Faculty of Medicine and Dentistry, Queen Mary University London, London, UK.

[4] Faculty of Land and Food Systems, Food, Nutrition & Health, University of British Columbia, BC, Canada

[5] School of Kinesiology, University of British Columbia, BC, Canada

[6] University of Miami Miller School of Medicine, Miami, FL, USA

[7] School of Kinesiology and Health Studies, Queens University, Kingston, ON, Canada

* Joint senior authors

Correspondence to: Jonathan C. Mcleod, Jonathan.mcleod@queensu.ca

ABSTRACT

A majority of human genes produce non-protein-coding RNA (ncRNA), and some have roles in development and disease. Neither ncRNA nor human skeletal muscle is ideally studied using short-read sequencing, so we used a customised RNA pipeline and network modelling to study cell-type specific ncRNA responses during muscle growth at scale. We completed five human resistance-training studies (n=144 subjects), identifying 61% who successfully accrued muscle-mass. We produced 288 transcriptome-wide profiles and found 110 ncRNAs linked to muscle growth *in vivo*, while a transcriptome-driven network model demonstrated interactions via a number of discrete functional pathways and single-cell types. This analysis included established hypertrophy-related ncRNAs, including *CYTOR* – which was leukocyte-associated (FDR = 4.9 $x10^{-7}$). Novel hypertrophy-linked ncRNAs included *PPP1CB-DT* (myofibril assembly genes, FDR = 8.15 x 10^{-8}), and *EEF1A1P24* and *TMSB4XP8* (vascular remodelling and angiogenesis genes, FDR = 2.77 x 10^{-5}). We also discovered that hypertrophy lncRNA *MYREM* shows a specific myonuclear expression pattern *in vivo*. Our multi-layered analyses established that single-cell-associated ncRNA are identifiable from bulk muscle transcriptomic data and that hypertrophy-linked ncRNA genes mediate their association with muscle growth via multiple cell types and a set of interacting pathways.

INTRODUCTION

Most genes in the human genome do not code for a protein [1] but instead are transcribed into non-coding RNAs (ncRNA), including long non-coding RNAs (lncRNA)[2]. Early work demonstrated that the proportion of ncRNA genes increases with organismal complexity [3], and it is now recognised that ncRNAs participate in many key biological roles [4,5], including regulating genome organisation and gene expression through nucleic and RNA–protein interactions [4,6]. Further, ncRNAs can act as a surveillance mechanism to prevent the accumulation of aberrant products of protein translation [7], participate in epigenetic regulation [8,9], and several ncRNAs are directly implicated in human diseases [6,10–13]. While ncRNAs classically have no-protein coding potential, emerging evidence suggests ncRNAs can harbour micro-peptides that have biological activity [14]. Nevertheless, most ncRNAs have no characterised function and are not reliably detected in human muscle using short-read sequencing [15], highlighting a need for their accurate measurement and biological characterisation.

Skeletal muscle accounts for ~40% of total body mass [16], is paramount in various mechanical and metabolic functions and is subject to age-related decline [17]. Resistance exercise training (RT) results in muscle fibre hypertrophy, mitigating ageing-related loss of muscle [18]. Yet not all humans robustly accrue skeletal muscle mass, even following prolonged supervised RT [19]. This lack of response is indicative that the influence of RT on growth is often not readily discernable beyond the technical variation of a measurement instrument [20]. Although exogenous factors – such as RT load or frequency [21] and ensuring adequate dietary protein provision [22] – modestly contribute to the load-induced hypertrophic phenotype, the intrinsic genomic characteristics of an individual are hypothesised to determine the bulk of the variability in hypertrophic response [23]. Early human studies stratifying RT-induced hypertrophy identified a paradoxical gene signature

consistent with less mammalian target of rapamycin complex 1 (mTORC1) activation in individuals with the greatest hypertrophy [24] or altered microRNA response profiles [19]. Ultimately, studying individuals with the most robust responses to muscle loading may yield novel insights into causal regulators of adaptation and potentially identify therapeutic targets for treating muscle loss, including sarcopenia [25].

The current understanding of exercise transcriptomics is mostly limited to protein-coding genes; however, ncRNAs have begun to emerge as critical regulators of skeletal muscle growth. Recently, Wohlwend and colleagues [26] identified the lncRNA cytoskeleton regulator RNA (*CYTOR*) as regulated during muscle growth, negatively regulated with age and one that promoted fast skeletal muscle fibre expression in mice by sequestering the TEA domain transcription factor 1 (*TEAD1*). We discovered that the lncRNA, *FRAIL1*, was increased with muscle age [27], and more recently, increased *FRAIL1* was found to negatively influence muscle strength and function [28]. Additionally, *Chronos* is a skeletal muscle-enriched lncRNA that was shown to repress hypertrophic growth in vitro and in vivo by negatively regulating Bmp7 expression [29]. Despite the emerging recognition that ncRNAs act as regulators of skeletal muscle development [30], myogenesis, and musculoskeletal disease [31], most ncRNAs have no known function in adult muscle [1]. The multi-nucleated and fibrous nature of skeletal muscle fibres makes it challenging to study using single-cell transcriptomics, and most single-cell technologies do not readily capture the noncoding transcriptome. In the present study, we generated five independent supervised exercise training studies (n=144 subjects) and applied our customised bulk RNA profiling strategy [13,27,32], which more reliably detects ncRNAs in human muscle [15]. Combined with pathway analyses [33,34], data-driven quantitative RNA network modelling [35] and

selective spatial profiling, we were able to localise ncRNAs to specific cell types within muscle, providing insight into their biological role [36,37].

METHODS

Description of five independent clinical studies. For a brief overview of the analysis, please refer to Figure 1. Each exercise intervention study utilised *supervised* training to load the thigh muscle and promote hypertrophy. It is known that a wide range of exercise protocols yield similar group average increases in muscle mass [20,21,24,38,39]. Accordingly, despite variations in training experience and training load, the relative gains in lean mass in each study demonstrated the same average increase. Note that the global transcriptome profiles were partially utilised (other than 50 new transcriptome profiles) to validate a list of 141 protein-coding genes identified during the remodelling of lean mass with altered loading [25]. All five studies were approved by local research ethics boards and complied with all ethical standards for research involving human participants set by the Declaration of Helsinki.

Study 1. Morton et al. [40] used recreationally active men (age: 22 ± 3 years; body mass index [BMI]: 26 ± 7 kg/m^2). Each participant's dominant leg was randomly assigned to a high-load, low-repetition (8-12 repetitions at ~70-80% 1-repetition maximum [1RM]), RT protocol or a low-load, high-repetition (20-25 repetitions at ~30-40% 1RM) RT protocol. The contralateral leg was assigned to the opposite condition providing two distinct interventions. Participants underwent RT three days a week (Monday, Wednesday, and Friday) for 10 weeks. Each RT session consisted of 3 sets of unilateral knee extensions to volitional fatigue (the starting leg alternated between RT sessions). RT-induced skeletal muscle hypertrophy did not differ between

allocation conditions. Participants also received 25 g of whey protein isolate supplement twice daily (morning or post-exercise and pre-sleep) for the duration of the study. A muscle biopsy was obtained at pre- and post-training for 32 participants. Unilateral leg lean mass (LLM) was quantified using dual-energy X-ray absorptiometry (DXA) pre- and post-training.

Study 2. Muscle biopsies originated from Morton et al. [39]. Participants were active, with 4 – 5 years of RT experience, and then performed RT 4 days/week (Mon, Tues, Thurs, Fri) for 12 weeks (all the major muscle groups). Each session included 5 exercises performed for 3 sets to volitional failure. Participants were randomly assigned to complete either low-load, high-repetition (20-25 repetitions per set at ~ 30% - 50% 1-RM) RT or high-load, low-repetition RT (8-12 repetitions per set at ~ 75%-90% 1-RM). Indices of muscle hypertrophy did not differ between the training groups. Participants consumed 30 g of protein after each exercise session. Biopsy tissue was available at baseline and following 12 weeks of RT for 33 participants. The average of bilateral LLM was assessed using DXA at pre and post training.

Study 3. Muscle biopsies originated from Phillips et al. [41]. Sedentary participants performed high-intensity cycle training 3 days per week (Monday, Wednesday, and Friday) for 6 weeks. Each session consisted of a 2 min warmup at 50 W followed by 5 sets of high-intensity cycling at 125% $VO_{2\ peak}$ for 1 minute. Each set was separated by 90 s of rest. Biopsy tissue was available at pre- and post-training for 47 participants, including 18 males and 29 females with an average age of 39 years (range 21-51 years) and a BMI of 31 kg/m^2 (range 26 - 43 kg/m^2). Unilateral upper LLM was assessed using DXA at baseline and 3 days following the final training session.

Study 4. Muscle biopsies originated from Mitchell et al. [42]. Young, recreationally active men participated in whole-body RT 4 days per week for 16 weeks. RT sessions consisted of two upper-body and two lower-body training sessions per week. The program progressed from 3 sets

of 12 repetitions to 4 sets of 6 repetitions of each exercise. The last set of each exercise was performed to volitional failure. Participants consumed 30 g of protein immediately after each exercise session. Biopsy tissue was available for 20 participants pre- and post-training. Unilateral thigh muscle volume was measured using Magnetic Resonance Imaging (MRI) pre- and post-training.

Study 5. Muscle biopsies originated from Stokes et al. [25]. Recreationally active men (age: 21 ± 3 years; BMI: 24 ± 3 kg/m^2) underwent unilateral leg extension and leg press RT thrice weekly (Monday, Wednesday, and Friday) for 10 weeks. Specifically, each session consisted of 3 sets of 8-12 repetitions of leg extension and 3 sets of 8-12 repetitions on a leg press. The last set of RT was performed to volitional failure. Following each exercise session, participants ingested 25 g of whey protein isolate. Biopsy tissue was available for 12 participants pre- and post-training. Unilateral LLM was measured pre- and post-training using DXA.

Defining hypertrophy beyond typical laboratory variation. Changes in DXA LLM (or, in one case, quadriceps muscle volume by MRI) defined subjects that demonstrated a genuine increase in muscle mass (‘responders’). For the remaining subjects, we could not show they demonstrated training-induced hypertrophy (we do not claim they have no response). We used the technical variation threshold for DXA-derived changes in LLM (2.0 – 2.4%) [43,44] and MRI-derived changes in thigh muscle volume (2.3%)[45] as cut-off values for these two groups. For all individuals, the percentage change in LLM (or quadriceps muscle volume for MRI) post-exercise training was calculated. Critically, there was no association between baseline LLM and changes in LLM (Figure S1; Table S1). Individuals who exhibited a ≥ 2.5% increase in LLM were defined as “LM Responders (LMR),” whereas individuals who showed < 2.0% change in LLM (or change in quadriceps muscle volume for [42]) were defined as having “No measurable LM

response (NMLMR)." These two groups (LMR N=88; NMLMR N=50) were studied separately for evidence of differential noncoding gene expression (DE). Only 6 individuals fell within the range of reported precision error (2.0 – 2.4%) of the DXA (or MRI), and they were included in the linear modelling analysis.

Clinical data for quantitative network modelling. We used n=437 transcriptome profiles from mainly sedentary subjects, aged 50y or younger, to generate a human muscle tissue gene co-expression model using multiscale embedded gene co-expression network analysis (MEGENA)[35]. A total of 35,079 protein-coding and non-coding genes were used as input, and the analysis time was *~600 hours* on a 3.2GHz 16-core Intel Xeon W-based Mac Pro (768GB 2933 MHz DDR4 RAM). Unlike most popular and fast network methods, MEGENA applies statistical thresholds to identify significant relationships at both the gene and network structure level, e.g. false discovery rate (FDR) < 1% for gene-gene Pearson correlation coefficients, $P < 0.05$ for module significance, $P < 0.01$ for network connectivity, with 1000 permutations for adjusted values (FDR). We present the overall hierarchical organisation of the planar filtered networks using a sunburst plot, and individual module plots were produced using Fruchterman-Reingold force-directed plotting within MEGENA [35]. Gene co-expression modules that contained our candidate ncRNA genes were labelled in the sunburst plot and studied further (See below).

RNA extraction and transcriptome profiling. In each case, RNA was extracted from approximately 20 mg of muscle tissue[25,39,40,42] in 1000 mL of TRIzol, which was added to Lysing Matrix D tubes containing ceramic microbeads (MP Biomedicals, Solon, OH, USA) and homogenised using a FastPrep tissue homogeniser (MP Biomedicals, Solon, OH, USA). 200 mL of chloroform was added, and the tubes were hand-shaken vigorously for 15 s and incubated at

room temperature for 5 min. Samples were then centrifuged at 12 000 g for 10 min at 4°C, and the upper aqueous phase containing RNA was transferred to an RNase-free tube. RNA was purified using the EZNA Total RNA Isolation kit (Omega Bio-Tek, Norcross, GA, USA). RNA was processed for transcriptome profiling using the GeneChip WT Plus Reagent Kit (no PCR) by processing to single-stranded sense DNA via a *reverse transcription linear priming strategy* that primes the poly-A and non-poly-A RNA. First and second-strand cDNA synthesis was performed using ~100 ng of RNA and a spike-in Poly-A control, followed by reverse transcription into cRNA. cRNA was purified using magnetic beads and quantified using spectrophotometry (Nanodrop UV-Vis, Thermo Fisher Scientific). 15 mg of cRNA was then amplified and hydrolysed using RNase H (leaving single-stranded cDNA) and purified with magnetic beads. cDNA (5.5 mg) was then fragmented, labelled, and hybridised to an array. The array was washed and stained using a GeneChip Fluidics Station 450 (Thermo Fisher) and scanned using a GeneChip Scanner 3000 7G (McMaster Genomic Core Facility, Hamilton). Samples from Phillips et al. [41] were processed using a Qiagen Tissuelyser and processed as above without the additional purification step (Jensen Laboratory, MPI, Horsholm, Denmark).

Computational processing of the HTA 2.0 array platform. We updated our 2017 process for annotating and processing the transcriptomic technology[13,15,25,27,46]. Briefly, the HTA 2.0 array has 6.9 million 25-mer probes and the annotation of each probe is checked against the recent reference genome and transcriptomes[47,48] using R. To do this, we produce a standardised FASTA (with a unique label for each 25mer probe) file, a probe GC content file and a probe-level chip definition file (CDF). For the present study, the FASTA file was aligned against Grch38 - Gencode 43 [49] using the STAR aligner [50]. Probes that uniquely map were combined to form groups of probes (probe-sets), and each probe-set relied on n>3 probes (median = 66). In

addition, the raw probe signal of a large number of diverse human muscle profiles (n=1124, GSE154846) was analysed using the probe-level CDF and aroma.affymetrix [47], affy [51] and the affxparser (bioconductor.org/packages/affxparser/) packages. Probes with both a very low signal and a low coefficient of variation were removed to arrive at a final set of probes to be included in the CDF [13,15,25,27,46]. This CDF was then used to summarise RNA expression from the GC-corrected CEL files produced from Studies 1-5 and 437 pre-existing CEL files, after which iterative rank-order normalisation (IRON) [52] in the default mode was used to generate a normalised expression matrix. From the starting 6.9M probes, reannotation and summarisation yielded a transcript level probe-set CDF used 5.23M probes to define 220.6K probe-sets prior to study-specific transcript signal filtering (Supplement Data S1). The custom CDF used in this study is deposited at GSE154846, along with new raw data produced for this study (GSE270823). This updated CDF can be utilised to extract any other human muscle data sets produced on the HTA 2.0 platform. We estimated that a total of 173,594 transcripts were annotated above the background signal using standard deviation-based filtering.

Differential expression analyses of ncRNA genes. For DE analyses, we used SAMR [53] and 10K permutations to estimate the false discovery rate (FDR), a method that appears more robust than other p-value correction methods [54]. Paired SAMR analyses were applied to the LMR group (176 paired RNA samples) and the NLMR group (100 paired RNA samples). We relied on an FDR cut-off of 5% and a ≥ |1.2| fold change to generate differentially expressed ncRNA lists. To focus on the most distinct observations between the LMR and NLMR groups, we applied the following heuristics. We prioritised ncRNA transcripts that displayed a fold change in opposite directions across our two response groups or where the differentially expressed ncRNA showed a fold change ratio between the groups ≥ |1.2|. Finally, to clarify if there were any ncRNAs

differentially expressed at baseline between our groups (note baseline physiology could not distinguish LMR and NLMR groups), we utilised an unpaired SAMR analysis (using the same criteria for a differentially expressed transcript as described above).

Assessing the relationship between changes in gene expression and changes in lean mass. The linear relationship between changes in ncRNA transcript expression and changes in LLM (or change in quadriceps muscle volume for [42]) was examined using a type III analysis of variance (R Core Team (2021). R: A language and environment for statistical computing. URL https://www.R-project.org/.). We used the following linear model: changes in ncRNA transcript ~ changes in LLM. A Pearson correlation coefficient (r) and a p-value were calculated for each transcript per study. Using the three largest cohort studies [39–41], we combined p-values using the Stouffer method, using the poolr R package [55]. For transcripts that passed filters 1 and 2 (see below), FDRs were calculated [56] using multtest [57]. ncRNA transcripts that were deemed to change linearly in proportion with delta lean mass passed all of the following filters: 1) 5-study median r (absolute) ≥0.2; 2) consistent (direction) r value in 4/5 studies; and 3) an FDR < 10% (the median was FDR 8%).

Cell type-specific gene markers and MERSCOPE-based transcript localisation. We calculated Pearson correlation coefficients and p-values (FDR adjusted) to establish the association of ncRNAs or gene co-expression modules with markers of type I and type II muscle fibres and rarer mononuclear cell types found in bulk skeletal muscle (satellite cells, endothelial cells, pericytes, macrophages, T-cells, and B-cells). These analyses relied on a network model generated using 437 muscle biopsy samples in individuals aged 50y or younger (GSE154846). We used the following myonuclei and mononuclear cell-specific gene markers: type I fibres (*MYH7, TNNT1*)[58–60], type II fibres (*MYH1, MYH2, ATP2A1, TNNT3*) [58–60], satellite cells (*PAX7,*

MYF5) [58,61], endothelial cells (*ENG, TIE1, PECAM1, APLNR*), pericytes (*RGS5, HIGD1B*) [58,62], macrophages (*F13A1, SPP1*) [58], T cells (*CD3D, IL7R*) [58,63], and B cells (*MS4A1, CD79A*) [58,63]. The MERSCOPE is a spatially resolved single-cell transcriptome profiling technology. As part of the process of designing and validating ongoing work in our laboratory, we produced images of the location of a small number of the ncRNAs identified in the present study. The MERSCOPE assay also included markers for muscle fibre types, satellite cells, and endothelial cells (type I fibre [MYH7 fish probe] [58–60], type II fibres [ATP2A1 fish probe] [58–60], satellite cells [PAX7, MYF5 merfish probes] [58,61] and endothelial cells [ENG, TIE1, PECAM1, APLNR merfish probes]). The panel was used to profile three independent muscle samples originating from the present study, and some ncRNA data pertinent to the present results is presented. The gene list was sent to Vizgen Inc, and they selected 30-50 merfish probes per gene for profiling on the MERSCOPE. Briefly, each fresh frozen sample embedded in the optimal cutting temperature compound (OCT, Tissue-Tek, The Netherlands) was sectioned at a thickness of 10 um in a cryostat at -20 °C and transferred onto the circular MERSCOPE glass slide (PN 2040001, Vizgen, USA) within the fiducial bead border, and prepared for transport [64,65]. Tissue sections were fixed in pre-warmed 4% paraformaldehyde for 1 hour at 37°C. After fixation, the tissue sections were washed in 1X PBS 3 times for 5 min at room temperature, permeabilised in 70% ethanol (molecular grade) at 4°C overnight. Then, Vizgen cell boundary staining kit (PN 10400009, Vizgen, USA) was applied to stain cell membranes on the tissue sections after a 1-hour incubation in Blocking Solution mixed with RNase inhibitor (PN 20300100, Vizgen, USA). Afterwards, the tissue sections were incubated with Formamide Wash Buffer (PN 20300002, Vizgen, USA) at 37°C for 30 min and incubated in the custom-designed merfish panel at 37°C for about 40h. Then, the slide was incubated in the Formamide Wash Buffer at 47°C (30 min ×2),

rinsed with the sample preparation buffer, and stained with the DAPI and poly(T) Staining reagents, and the fiducial fluorescent beads (perimeter of scannable area). The probes were imaged using the MERSCOPE (Vizgen Core Laboratory, Boston, USA) with default settings (poly(T) and DAPI and Cell Boundary Channels "on", while scan thickness was 10μm). The raw images were converted to "vzg" meta-output files. For ncRNAs included in both assays, we used the MERSCOPE visualiser software and cell-specific marker probes to evaluate the location of each ncRNA.

Functional enrichment pathway analysis. Enrichment analyses (e.g., gene ontology) [33] are used to uncover the functional biology of lists of genes, categorising genes by their known biochemical functions [66]. For each network module, enrichment analysis was executed using the web tool Database for Annotation, Visualisation, and Integrated Discovery (DAVID; https://david.ncifcrf.gov/) [33], versus a custom background file containing the protein-coding genes estimated to be expressed in skeletal muscle tissue in the present study [66]. Most ncRNAs are not ontologically characterised and thus do not contribute to the enrichment analyses. Data-driven RNA network modelling methods are constructed based on experimentally derived gene co-expression similarities[35], and so provide a solution to categorising ncRNAs using "guilt by association". Gene co-expression modules with less than 500 genes and gene ontology (GO) terms with an FDR $\leq 5.0\text{x}10^{-5}$ were selected for further study. The gene lists from the ncRNA-containing modules, along with the background list of expressed genes, were analysed using the compareCluster function[67,68] in the ClusterProfiler R package utlising the GOTERM_BP_ALL from DAVID. ClusterProfiler was used to carry out functional enrichment using over-representation analyses and combined with enrichment mapping[67] to establish links between

distinct ncRNA-containing MEGENA modules. Note that not all gene identifiers from each module are mapped to the databases being used to generate these pathway analyses (a common problem).

RESULTS

Skeletal muscle hypertrophy following supervised exercise training. The average change in LLM (using DXA) across [25,39–41] was 3.4 ± 3.9% (range: -4.9 % to 18.8%); the average change in quadriceps muscle volume using MRI [42] was 7.1 ± 7.0% (range: -1.8% to 24.7%). Out of 144 participants, 88 individuals (61% of the total sample) were defined as LMR, whereas 50 individuals (34% of the total sample) did not demonstrate LLM changes beyond typical measurement error (NMLMR group). Thus, the average change in LLM for the LMR group and the NMLMR group was 6.6 ± 3.9% (range: 2.5% to 24.7%) and -0.6 ± 1.8 % (range: -4.9% to 1.9%), respectively (Figure 2). Baseline LLM status could not explain the observed variation in LLM gain (Figure S1; the demographics of the individual studies can be found in Table S1). We do not claim that the NMLMR subjects can not grow muscle tissue, just that we are unable to unequivocally assign any change in LLM beyond previously established method variation and we treated them as phenotypically divergent on this basis.

Overview of RNA molecules measured in bulk human skeletal muscle using high-density arrays. 58% of quantified genes were protein-coding after filtering out low signal (n=13249, Figure 3A). The majority of detectable ncRNA genes in skeletal muscle are annotated as "lncRNA" molecules (7173 genes), which are broadly categorised as genes that are ≥ 200bp in length. Other classes of ncRNAs included miscellaneous RNA (n=1192; ncRNA genes that are <200bp in length) and pseudogenes (n=1254). Note that ncRNA genes are routinely described as

'low-abundance' genes [36] based on sequencing cDNA libraries. We find here that the expression profile of ncRNA genes is similar to protein-coding genes in human skeletal muscle (Figure 3B) using a library preparation method that does not rely on PCR and is not 3' biased - consistent with a previous meta-analysis [15] from our group. The superior coverage with our array protocol over typical sequencing protocols most likely reflects, firstly, a more diverse cRNA library and, secondly, the lack of use of a competitive/counting quantification method, enabling more equitable detection of all RNA species (where array probes exist for that RNA – which in practice results in substantial greater coverage of the muscle transcriptome[15]).

Establishing a set of ncRNA genes related to skeletal muscle hypertrophy. One hundred ninety-three ncRNA genes were significantly regulated in the LMR group (Supplement Data, S2), whereas 50 genes were significantly regulated in the NMLMR group (Supplement Data, S3). To enable us to focus on the most robust results, we applied heuristic filtering (see Methods) to identify those ncRNA that demonstrated the most distinct pattern of regulation between our two groups[13,69,70]. This analysis revealed a subset of 50 ncRNA genes that were specifically regulated just in the LMR group and so may be directly linked with hypertrophy. Fifteen ncRNA genes were uniquely regulated in the NMLMR group (Figure 3C), and these may be associated with processes that impair growth or aim (unsuccessfully) to overcome negative influences on growth.

Notably, only two ncRNA genes were differentially expressed between the two groups prior to supervised training (Supplement Data S4), demonstrating that these baseline ncRNA transcriptomic profiles, much like the physiological characteristics, did not distinguish LMR from NMLMR groups (Figure 3D). In addition to DE analyses applied to the two post-hoc categorical groups (i.e., LMR group vs NMLMR group), linear analysis was used to determine if

there was a linear relationship between changes in ncRNA gene expression and changes in LLM, using all 144 subjects. This analysis identified 46 ncRNA genes with a modest relationship to gain in LLM (median r= 0.26; median FDR = 8%; Figure S2A; Supplement Data S5). Combined with the DE analyses, a final list of 110 hypertrophy-related ncRNA genes (Supplement Data S6) was considered further. Notably, we identified most of the known muscle hypertrophy-related ncRNA genes (e.g. *CYTOR*, *MYREM*, *H19*, and *MEG3*), which now have some established biochemical roles in skeletal muscle (Table S2). The rest of the hypertrophy ncRNAs had no prior associated function in skeletal muscle (Table S2). Cardiac mesoderm enhancer-associated non-coding RNA (*CARMN)* was the only ncRNA gene that displayed a linear association with changes in LLM (Figure S2B-F) *and* was differentially expressed in the LMR group. Critically, only 30% of the hypertrophy ncRNA genes are consistently detected in skeletal muscle by RNA sequencing [71,72] (Figure 3E; Supplement Data S7), and only five ncRNA genes (*CASC15*, *MYREM*, *DANCR*, *MIR4435-2HG*, *MEG3*) were reported as being regulated by RT when using RNAseq [72].

Spatial distribution of ncRNA genes in human skeletal muscle. There are several multi-plex true single-cell spatial technologies[64,65,73], and we present here data from the MERSCOPE single-cell spatial workflow to provide the visual location of a few hypertrophy ncRNA genes, along with markers of type I and type II muscle fibres, satellite cells and endothelial cells [58]. The prototype MERSCOPE assay (for an overview of the 3 samples used for MERSCOPE-MERFISH, please refer to Figure S3) showed reasonable agreement with the bulk expression data from the same biopsy sample (r = 0.78 – 0.81). In our bulk transcriptomic data, *MYREM* (*MYBPC2* cis regulating lncRNA enhancer of myogenesis (ENSG00000268518)) expression was positively associated with type II fibre markers (e.g., *TNNT3*: r =0.37; FDR = 2.57 x10^{-14}; Figure

4A) [58], and negatively associated with type I fibre markers (e.g., *MYH7:* r = -0.33; FDR = 1.45 x10^{-11}; Figure 4A) [58]. Visually, *MYREM* is concentrated beneath the basal lamina and was not observed in nuclei with gene markers of satellite cells (*PAX7, MYF5*) or endothelial cells (*APLNR, TIE1, KDR, ENG*), indicating that *MYREM* is a novel marker of mature myofibril nuclei in humans (Figure 4B), especially in type II fibres. This interpretation is supported by recent data from Chang and colleagues [74] demonstrating that *MYREM* increases the transcriptional expression of *MYBPC2*, a type II isoform of skeletal muscle myosin-binding protein C [75,76].

H19 is an imprinted lncRNA, and its pre-training abundance in human muscle is associated with training-induced changes in maximal aerobic capacity [77]. Spatially, it was ubiquitous throughout human skeletal muscle (Figure 4C) without any strong associations with fibre type markers or mononuclear cell types (Figure 4A). In contrast, Maternally Expressed Gene 3 (*MEG3)*, another imprinted lncRNA, was co-localized with satellite cell gene markers (*PAX7* and *MYF5*; Figure 4D), and its expression was significantly correlated with *PAX7* expression (r =0.51; FDR = 2.48 x10^{-29}; Figure 4A) in the bulk transcriptomic data. Indeed, a previous report in mice [78] found that *MEG3* is enriched in satellite cells and modulates myoblast differentiation and proliferation, impacting skeletal muscle regeneration.

Cardiac mesoderm enhancer-associated non-coding RNA (*CARMN*) had a low average expression in bulk human skeletal muscle (4.4 $\log_2$ units), implying it may not be expressed by mature muscle cells. Figure 4E demonstrates that *CARMN* appears located near endothelial cell gene markers (*APLNR, TIE1, KDR, ENG*), and we noted that it was positively associated with endothelial cell gene markers (e.g., *TIE1*: r =0.33; FDR = 3.26 x10^{-12}; Figure 4A) in our bulk transcriptomic data. Previous work claimed that *CARMN* is a vascular smooth muscle cell-

specific lncRNA [79]. Although vascular smooth muscle cells are absent from muscle capillaries [62], pericytes are associated with endothelial cells in skeletal muscle and have been proposed to regulate endothelial cell proliferation and differentiation [80]. Notably, in our data, *CARMN* expression is most strongly associated with pericyte gene markers (e.g., RGS5: r =0.50; FDR = 4.31 $x10^{-27}$; Figure 4A), which leads us to hypothesize that *CARMN* might modulate the role of pericytes during skeletal muscle growth. Many reports of cell-unique patterns of lncRNA expression come from a failure to appreciate the limitations of RNAseq cDNA library production[81]. Like *CARMN* expression, cancer susceptibility candidate 15 (*CASC15*) also has a low signal in bulk skeletal muscle (Figure 4E). *CASC15* is an intergenic lncRNA, and small interfering knockdown experiments have shown that *CASC15* contains tumour-promoting properties in melanoma cell lines [82], and we find greater expression of *CASC15* is associated with human muscle growth *in vivo*.

Data-driven RNA network modelling of ncRNA and protein-coding genes demonstrates that the hypertrophy-related ncRNAs represent functionally interacting pathways. Given most ncRNAs have no known function despite representing half the genome, inference methods are required to highlight potential molecular functions. We applied time-consuming data-driven quantitative network modelling to the muscle coding and noncoding transcriptome (n=437) and identified statistically robust co-expression modules that contained hypertrophy-related ncRNAs. There were 136 significant co-expression modules that contained at least one hypertrophy-related ncRNA (Figure 5A). Twelve of these modules were enriched in gene ontology biological processes, including cell migration, contractile fibre, inner mitochondrial membrane complex, RNA processing, and MHC protein complex processes (Table 1; Supplement Data S8 - 10). Application of a network-based enrichment method[68] to the co-expression modules

independently identified by MEGENA, in independent data, identifies that the hypertrophy ncRNA-containing modules interact at least two levels (Figure 5B). Firstly, genes belonging to modules contribute to more than one distinct biological function (pie-chart structures) both within and across functional groups (e.g. regulation of cell activation and positive regulation of cytokine production). Secondly, functional group labels highlight muscle tissue level processes (e.g. muscle structural development and vascular development) or the involvement of low abundance cells (e.g. lymphocyte activation). The genes driving these significant overlapping interactions are listed in Supplement Data S11.

We next explored, in fine detail, some of the key MEGENA modules. One containing 60 genes included *CYTOR* – a ncRNA known to regulate hypertrophy in model systems - (Figure 6A; Table 1) – and the module represented immune-related processes e.g. leukocyte migration (FDR = 1.05×10^{-6}; fold enrichment [FE] = 10.61), lymphocyte activation (FDR = 4×10^{-7}; FE = 6.62), and leukocyte chemotaxis (FDR = 1.56×10^{-5}; FE = 13.42). The hub gene of this module was lymphocyte cytosolic protein 1 (*LCP1*, or L-plastin), which has a direct role in aggregating actin filaments into parallel bundles, which is critical for T-cell activation, migration, and stability [83]. *LCP1* expression was positively correlated with *CYTOR* expression (r = 0.49) in the bulk muscle transcriptome (Figure S3A). *FCER1G*, which encodes the Fc Epsilon Receptor Ig protein, facilitates the activation of natural killer cell lymphocytes, and it was also positively correlated with *CYTOR* (r = 0.66; Figure S4A). The median expression of the network genes in skeletal muscle is very low (3.7 $\log_2$ units; Figure 6B), indicating that this module of co-expressed genes is likely expressed in the small number of immune cells found in muscle tissue – illustrating the sensitivity of our transcriptomic methods. To further investigate, we reprocessed publicly available data from the same laboratory platform, obtained from human primary

immune cells (macrophages [GSE124106], CD8+ T cells [GSE117230], and CD4+ T cells [GSE62921], endothelial cells [GSE236137], and our own *in vitro* human myotube data [27]. We noted that *LCP1*, *FCER1G*, and *SLC31A2* are mostly expressed in immune cells (macrophages, CD8+ and/or CD4+ T-cells), compared with other cell types found in skeletal muscle tissue samples (Figure 6C). This trend is observed for most genes in the *LCP1* module (Figure S4B). Thus, *CYTOR* regulation is linked to successful muscle hypertrophy in humans and is found in an immune-cell-related module.

The next module investigated (Figure 7A; Table 1) centred around the slow skeletal muscle troponin isoform, *TNNT1*. This module was composed of genes robustly co-expressed in muscle cells, median expression of 6.4 $\log_2$ units (Figure 7 and Figure S5). Nested within this module was a hypertrophy-related ncRNA gene, phosphatase 1 catalytic subunit beta divergent transcript (*PPP1CB-DT*; Figure 7A). Based on DAVID analyses, the module was enriched in biological processes related to myofibril assembly (FDR = 8.15 x 10^{-8}; FE = 47.52), striated muscle contraction (FDR = 8.15 x 10^{-8}; FE = 47.52), muscle filament sliding (FDR = 8.15 x 10^{-8}; FE = 22.5), and the ontology label ‘transition between fast and slow fibre’ (FDR = 2.80 x 10^{-7}; FE = 217.81) above the muscle transcriptome. Attractin-like-1 (*ATRNL1*) is in this module, and we previously identified [25] *ATRNL1* was correlated with human skeletal muscle growth in a targeted analysis. The module also contained estrogen-related receptor gamma (*ESRRG*), which contributes to exercise-mediated remodelling of skeletal muscle function[84,85]. In mouse models, *ESRRG* promotes an increased number of oxidative muscle fibres and is considered a regulator of oxidative metabolism [86]. The expression levels of most genes in this module are positively associated with markers of type I fibres and negatively associated with markers of type II fibres

(Figure S5C). Collectively, the *TNNT1* module most likely reflects genes that enhance the oxidative capacity of skeletal muscle, a common occurrence with RT in humans [87,88].

A final module we considered in detail (370 genes; Figure 8; Table 1; Supplement Data, S9-10) was centred around *MAN1A1* and the *ATLASTIN GTPase 3 (ATL3)* genes, the latter of which are a constitutive endoplasmic reticulum fusion protein[89]. Loss of function mutations in *ATL3* lead to muscle weakness[90]. This large module was enriched in GO terms related to microvascular remodeling e.g., angiogenesis (FDR = 2.77 x 10^{-5}; FE = 3.55), blood vessel development (FDR = 6.36 x 10^{-8}; FE = 2.97), regulation of vasculature development (FDR = 1.66 x 10^{-6}; FE = 3.71), and circulatory system development (FDR = 1.66 x 10^{-8}; FE = 2.55). Network-based enrichment analysis[68] identified that these processes were directly linked to the muscle remodelling pathways. *EEF1A1P24* and *TMSB4XP8* are two hypertrophy-related ncRNA genes in this module, and both are pseudogenes (Figure 8; purple). Interestingly, they are part of a correlative cluster of several other pseudogenes (median R = 0.60; *EEF1A1P9, EEF1A1P17, EEF1A1P25, EEF1A1P22, EEF1A1P16, EEF1A1P6, TMSB4XP4, TMSB4XP2*; Figure 8 box inset). Pseudogenes are defined as copies of parent genes that are either retro-transposed counterparts or processed mRNAs (i.e., processed pseudogenes) or harbour mutations derived from gene duplication (i.e., unprocessed pseudogenes) [91]. In recent years, these genes have been identified as potential decoys for microRNAs and modulators of the sensitivity of the related protein-coding genes to inhibition [92].

DISCUSSION

The present study is a comprehensive profile of the human skeletal muscle ncRNA transcriptome, which successfully identified numerous hypertrophy ncRNA candidates embedded in tissue growth pathways, often in a cell-specific manner and that they represent modules of integrated overlapping pathways. Most of the 110 ncRNA genes linked to successful hypertrophy would not have been identified had we relied on a typical RNA sequencing workflow. The use of data-driven quantitative RNA network modelling in independent data, along with network-based pathway enrichment and single-cell spatial transcript profiles allowed us to identify the functional pathways and cell types these ncRNA genes operated within. We established that type II myofibril-associated *MYREM* demonstrates specific myonuclear domain expression *in vivo* in human muscle. This work also added to the growing body of evidence that local immune-related responses, mitochondrial remodelling, and angiogenesis are all critically important contributors to successful human skeletal muscle hypertrophy [23,93,94].

The benefits of high-density array profiling to study the skeletal muscle ncRNA transcriptome

A majority of recent skeletal muscle transcriptome studies have relied on short-read RNA sequencing [28,71,72,95–98]. We have shown that short-read RNA sequencing profiling of human skeletal muscle detects only ~20% of constitutively expressed ncRNAs and demonstrates enormous inter-study heterogeneity [71,72] (See Figure 3E). In the present study we estimate that >7000 ncRNA genes are detected in every skeletal muscle sample (Figure 3A), consistent with our previous work[13,15,27,46]. Notably, only 30% of the 110 hypertrophy ncRNA genes were consistently detected in two short-read RNA sequencing studies of skeletal muscle growth (Figure 3E). Stochastic properties of sequencing and the reliance on poly-A enrichment strategies (ncRNAs are deficient in poly-A tails) means that most ncRNAs are not detected. A striking example is *H19*, a hypertrophy and exercise-related ncRNA that is abundantly expressed in

human skeletal muscle (Supplement Data, S8), yet a recent RNA sequencing study indicated that H19 was not 'robustly expressed' in human skeletal muscle [28]. In 2012, we identified *H19* as being part of a baseline gene expression signature predictive of the cardiovascular adaptive response to exercise training [77]. More recent work demonstrated that the *H19* locus encodes several miRNAs that regulate protein translation initiation factors implicated in protein synthesis [99]. Interestingly, *H19* directly interacts with the C-terminal domain of dystrophin, blocking its degradation [100]. Dystrophin links the internal cytoskeleton to the extracellular matrix [101], and transcriptome responses to exercise are linked to Dystrophin status [69]. In Duchenne Muscular Dystrophy (DMD), *H19* interaction with dystrophin is impaired, resulting in the degradation of dystrophin and muscle degeneration [100]. Clearly, all of this evidence indicates that *H19* is a crucially important lncRNA in muscle (with wide-spread expression; Figure 4C) and directly contributes to regulating tissue remodelling.

Identifying the spatial localisation of ncRNA genes aids in generating functional hypotheses

Skeletal muscle is a conglomeration of cells dominated by large multinucleated myofibers while containing mononucleated cells, including satellite cells, endothelial cells, immune cells, and pericytes. There is growing support that these rarer cells contribute to skeletal muscle remodelling and that perturbation of their role is related to muscle dysfunction [58,102,103]. Using merfish probes, we illustrated that our hypertrophy ncRNA *MYREM* was localised near the periphery of skeletal muscle fibres and co-stained with DAPI indicative of mature myonuclei [104]. Previous *in vitro* work showed that *MYREM* was markedly abundant in the nuclei of myotubes compared with the nuclei of myoblasts [37]. Our data indicate that *MYREM* appears to be a novel marker of human myonuclei *in vivo* (absent from cells expressing endothelial or satellite cell marker genes). Nuclear lncRNAs participate in vital processes, such as chromatin organisation,

transcriptional regulation, and RNA processing [105]. *MYREM* interacts with the RNA-binding protein (RBP), heterogeneous nuclear ribonucleoprotein L (HNRNPL) to enhance the transcription of the fast-twitch isoform skeletal muscle myosin-binding protein C2 (*MYBPC2*). *MYBPC2* is involved during the later stages of the myogenic program, whereby mononucleated myoblasts fuse into multinucleated myotubes, and the myosin heavy chain proteins are expressed and function in muscle contraction [106]. Interestingly, network modelling indicated that *MYREM* is co-expressed with a mitochondrial-inner membrane gene expression module (Figure S6) containing genes such as *ATP5F1D*, *NDUFA3*, but also the protein-translation initiation factor *EIF3K* [107]. Remodelling of the mitochondria during hypertrophy-induced myogenesis may support increased energetic-related mechanisms (e.g., translation[108]), explaining why a myogenesis lncRNA is co-expressed with mitochondrial-related genes and given this may mostly reflect the physiological loading of type II muscle fibres.

To our knowledge, we are the first to report that *MEG3* localises rather selectively to muscle satellite cells in human skeletal muscle (Figure 4D), while *MEG3* has been reported to be nuclear located in other cell types [37]. *MEG3* is a maternally imprinted gene known to have tumour-suppressive properties in various cancers [109]. Interestingly, *Gtl2*, the mouse ortholog of *MEG3* [110], targets the polycomb repressive complex 2 to epigenetically silence a variety of genes from the *Dlk1-Dio3* locus, including the protein-coding transmembrane gene, *Dlk1* [111]. A muscle-specific *dlk1* knockout in mice has altered satellite cell lineage progression following skeletal muscle injury [112], and overexpression of *dlk1* is associated with pathological hypertrophy [113,114]. Taken together, the spatial location, network and whole tissue bulk correlation analysis indicates that several hypertrophy-related ncRNA genes in skeletal muscle are likely mediating their influence via rare cell types (by abundance) in skeletal muscle.

Data-Driven Network Analysis Provides Biological Insight into Novel ncRNAs

Most of the hypertrophy-related ncRNAs in the present study had no previous roles in skeletal muscle biology (Table S2). For example, *PPP1CB-DT* was co-expressed in a module of genes related to contractile fibre remodelling (Figure 7). *PPP1CB-DT* is a divergent ncRNA to *PPP1CB*, a protein-coding gene for one of three catalytic subunits of protein phosphatase 1 (*PP1*), which is a serine/threonine-specific protein phosphatase that plays major roles in regulating skeletal muscle contractility [115]. Divergent ncRNAs are transcribed in the opposite direction from the promoters of protein-coding genes [116] and may affect adjacent protein-coding genes through direct regulation in *cis* [117] or by participating in chromatin modifications [118]. We also noted that a pair of hypertrophy-related pseudogenes, *EEF1A1P24* and *TMSB4XP8*, were found to be regulated in a vascular remodelling and angiogenesis module (Figure 8). The angiogenic molecular program is tightly coupled to skeletal muscle growth [25,119], and enhancing angiogenesis (by aerobic conditioning) may augment growth [120]. *TMSB4XP8* is a thymosin beta 4-X (*TMSB4X*) pseudogene, an actin-binding protein with known roles in cell migration and angiogenesis [121]. In addition, *EEF1A1P24* is a processed pseudogene for the protein-coding gene, eukaryotic elongation factor 1 (*EEF1A*), which plays an important role in delivering the amino-acyl tRNA to the ribosome during protein synthesis [122]. Until recently a broad misunderstanding is that pseudogenes are non-functional counterparts to their related genes [91]. Pseudogenes exert biological functions in a DNA (facilitating chromatin structure remodelling or gene conversion [91]), RNA (competitive endogenous RNA networks [123]), and/or via protein (some pseudogenes contain protein-coding potential [6]) dependent manner. We demonstrated, using network-based pathway modelling on large-scale quantitative network models of independent muscle transcriptomes (n=437), that a group defined as ‘blood muscle morphogenesis and

development' directly connected the angiogenesis MEGENA modules with muscle tissue development (Figure 5B). These vascular-related ncRNAs may aid modification of microvascular flow during exercise [124] or feeding[125], which helps contribute to meeting the demands of increased rates of protein synthesis and overall a key role for the vascular system modulating muscle hypertrophy is now apparent [25,119,120].

RNA networks reveal novel roles of ncRNA genes in skeletal muscle immunomodulation

The immune system also appears to be a novel regulator of skeletal muscle remodelling[103]. Our ncRNA analyses highlight biological processes distinct from our previously described protein-coding hypertrophy signature [25], such as immune-cell-related functions (Figure S7). For example, *MIR4435-2HG* (a miRNA host gene) was co-expressed in a module dominated by immune-related processes (e.g., peptide antigen assembly with MHC class II protein complex; Table 1; Supplement Data, S10), and *MIR4435-2HG* has most recently described as a gene called '*Morrbid*'. *Morrbid* tightly regulates the lifespan and turnover of myeloid cells (e.g., neutrophils and eosinophils) by regulating the transcription of pro-apoptotic genes [95,126]. Notably, *CYTOR* was also co-expressed in an immune-dominated protein-coding RNA module (Figure 6), with robust expression in macrophages, CD8+ T cells, and CD4+ T cells (Figure S4B). To date, the characterisation of *CYTOR* in mouse muscle tissue has focused on muscle cells and not other cell types found within muscle tissue [95]. In muscle cells, *CYTOR* sequesters the *TEAD1* transcription factor [95], which can transcriptionally regulate the small peptide apelin that regulates paracrine communication between muscle cells and endothelial cells [127]. Apelin is a feature of the protein-coding pathways associated with human muscle growth. We find that *CYTOR* was widely expressed across multiple cell types (Figure 6C), suggesting that *CYTOR* can impact skeletal muscle hypertrophy via multiple mechanisms. The present analysis suggests a model whereby a

number of rare but important resident secretory cell types may regulate adaptation and release factors in a paracrine manner (e.g. a non-muscle source for various proposed myokines) to promote skeletal muscle remodelling [103]. Collectively, our analyses reveal that low-abundance cell types can be directly studied in bulk transcriptomic profiles of human skeletal muscle tissue.

LIMITATIONS

The present human clinical studies are not without its limitations. Four out of the five exercise loading studies relied on DXA to quantify changes in LLM, and the hydration status of the participant can influence this measure and contribute to the clinical variation[128] and this may have reduced our ability to identify ncRNA hypertrophy candidates. With respect to the interpretation of our results, although ncRNAs are predicted to contain no protein-coding potential, some ncRNAs contain small open reading frames that encode peptides [6,12]. Without additional experiments, some of the hypertrophy-related ncRNAs identified in the current study may also reflect the actions of novel bioactive peptides. Nonetheless, detailed mechanistic studies will be required to establish the direct involvement of each ncRNA in the hypertrophic response. Nevertheless, the few ncRNAs known to have causal links to cell growth and muscle tissue hypertrophy were identified by our methodologies.

ACKNOWLEDGEMENTS

JCM was supported by a Queens University Vice Principal Research Postdoctoral Fund. This work was also supported by Medical Research Council, UK through grants G1100015 and MR/Y010329/1 (JAT) and by the National Institutes of Health, USA (1R56AG061911-01 (CW and JT). This work was also funded by a grant to SMP from the National Science and

Engineering Research Council (NSERC) of Canada. SMP is supported by the Canada Research Chairs Program.

REFERENCES

1. Amaral P, Carbonell-Sala S, De La Vega FM, et al. The status of the human gene catalogue. *Nature*. 2023;622(7981):41-47. doi:10.1038/s41586-023-06490-x

2. Clark MB, Amaral PP, Schlesinger FJ, et al. The reality of pervasive transcription. *PLoS Biol*. 2011;9(7):5-10. doi:10.1371/journal.pbio.1000625

3. Liu G, Mattick J, Taft RJ. A meta-analysis of the genomic and transcriptomic composition of complex life. *Cell Cycle*. 2013;12(13):2061-2072. doi:10.4161/cc.25134

4. Mattick JS, Amaral PP, Carninci P, et al. Long non-coding RNAs: definitions, functions, challenges and recommendations. *Nat Rev Mol Cell Biol*. 2023;24(6):430-447. doi:10.1038/s41580-022-00566-8

5. Ugalde AP, Roiz-Valle D, Moledo-Nodar L, Caravia XM, Freije JMP, López-Otín C. Noncoding RNA Contribution to Aging and Lifespan. *J Gerontol A Biol Sci Med Sci*. 2024;79(4). doi:10.1093/gerona/glae058

6. Qian SH, Chen L, Xiong YL, Chen ZX. Evolution and function of developmentally dynamic pseudogenes in mammals. *Genome Biol*. 2022;23(1):235. doi:10.1186/s13059-022-02802-y

7. Kesner JS, Chen Z, Shi P, et al. Noncoding translation mitigation. *Nature*. 2023;617(7960):395-402. doi:10.1038/s41586-023-05946-4

8. Gutbrod MJ, Martienssen RA. Conserved chromosomal functions of RNA interference. *Nat Rev Genet*. 2020;21(5):311-331. doi:10.1038/s41576-019-0203-6

9. Pastori C, Kapranov P, Penas C, et al. The bromodomain protein BRD4 controls HOTAIR, a long noncoding RNA essential for glioblastoma proliferation. *Proc Natl Acad Sci U S A*. 2015;112(27):8326-8331. doi:10.1073/pnas.1424220112

10. Zhang F, Lupski JR. Non-coding genetic variants in human disease: Figure 1. *Hum Mol Genet*. 2015;24(R1):R102-R110. doi:10.1093/hmg/ddv259

11. Butler AA, Johnston DR, Kaur S, Lubin FD. *Long Noncoding RNA NEAT1 Mediates Neuronal Histone Methylation and Age-Related Memory Impairment*. Vol 12.; 2019. http://stke.sciencemag.org/

12. Lee C, Zeng J, Drew BG, et al. The mitochondrial-derived peptide MOTS-c promotes metabolic homeostasis and reduces obesity and insulin resistance. *Cell Metab*. 2015;21(3):443-454. doi:10.1016/j.cmet.2015.02.009

13. Timmons JA, Atherton PJ, Larsson O, et al. A coding and non-coding transcriptomic perspective on the genomics of human metabolic disease. *Nucleic Acids Res*. 2018;46(15):7772-7792. doi:10.1093/nar/gky570

14. Yeasmin F, Yada T, Akimitsu N. Micropeptides encoded in transcripts previously identified as long noncoding RNAs: A new chapter in transcriptomics and proteomics. *Front Genet*. 2018;9(APR):1-10. doi:10.3389/fgene.2018.00144

15. Stokes T, Cen HH, Kapranov P, et al. Transcriptomics for Clinical and Experimental Biology Research: Hang on a Seq. *Advanced Genetics*. Published online June 2023:2200024. doi:10.1002/ggn2.202200024

16. Janssen I, Heymsfield SB, Wang Z, Ross R. Skeletal muscle mass and distribution in 468 men and women aged 18–88 yr. *J Appl Physiol*. 2000;89(1):81-88. doi:10.1152/jappl.2000.89.1.81

17. Timmons JA. Molecular Diagnostics of Ageing and Tackling Age-related Disease. *Trends Pharmacol Sci*. 2017;38(1):67-80. doi:10.1016/j.tips.2016.11.005

18. McKendry J, Stokes T, McLeod JC, Phillips SM. Resistance Exercise, Aging, Disuse, and Muscle Protein Metabolism. *Compr Physiol*. 2021;11(3):2249-2278. doi:10.1002/cphy.c200029

19. Davidsen PK, Gallagher IJ, Hartman JW, et al. High responders to resistance exercise training demonstrate differential regulation of skeletal muscle microRNA expression. *J Appl Physiol*. 2011;110(2):309-317. doi:10.1152/japplphysiol.00901.2010

20. Lixandrão ME, Bamman M, Vechin FC, et al. Higher resistance training volume offsets muscle hypertrophy nonresponsiveness in older individuals. *J Appl Physiol*. 2024;136(2):421-429. doi:10.1152/japplphysiol.00670.2023

21. Currier BS, Mcleod JC, Banfield L, et al. Resistance training prescription for muscle strength and hypertrophy in healthy adults: a systematic review and Bayesian network meta-analysis. *Br J Sports Med*. 2023;57(18):1211-1220. doi:10.1136/bjsports-2023-106807

22. Morton RW, Murphy KT, McKellar SR, et al. A systematic review, meta-analysis and meta-regression of the effect of protein supplementation on resistance training-induced gains in muscle mass and strength in healthy adults. *Br J Sports Med*. 2018;52(6):376-384. doi:10.1136/bjsports-2017-097608

23. Roberts MD, McCarthy JJ, Hornberger TA, et al. Mechanisms of mechanical overload-induced skeletal muscle hypertrophy: current understanding and future directions. *Physiol Rev*. 2023;103(4):2679-2757. doi:10.1152/physrev.00039.2022

24. Phillips BE, Williams JP, Gustafsson T, et al. Molecular Networks of Human Muscle Adaptation to Exercise and Age. *PLoS Genet*. 2013;9(3). doi:10.1371/journal.pgen.1003389

25. Stokes T, Timmons JA, Crossland H, et al. Molecular Transducers of Human Skeletal Muscle Remodeling under Different Loading States. *Cell Rep*. 2020;32(5):107980. doi:10.1016/j.celrep.2020.107980

26. Wohlwend M, Laurila PP, Williams K, et al. The exercise-induced long noncoding RNA CYTOR promotes fast-twitch myogenesis in aging. *Sci Transl Med*. 2021;13:7367. https://www.science.org

27. Timmons JA, Volmar CH, Crossland H, et al. Longevity-related molecular pathways are subject to midlife “switch” in humans. *Aging Cell*. 2019;18(4):1-10. doi:10.1111/acel.12970

28. Miller MJ, Gries KJ, Marcotte GR, et al. Human myofiber-enriched aging-induced <scp>lncRNA</scp> *FRAIL1* promotes loss of skeletal muscle function. *Aging Cell*. 2024;23(4). doi:10.1111/acel.14097

29. Neppl RL, Wu CL, Walsh K. lncRNA Chronos is an aging-induced inhibitor of muscle hypertrophy. *Journal of Cell Biology*. 2017;216(11):3497-3507. doi:10.1083/jcb.201612100

30. Biferali B, Mocciaro E, Runfola V, Gabellini D. Long non-coding RNAs and their role in muscle regeneration. In: ; 2024:433-465. doi:10.1016/bs.ctdb.2024.02.010

31. Ballarino M, Morlando M, Fatica A, Bozzoni I. Non-coding RNAs in muscle differentiation and musculoskeletal disease. *Journal of Clinical Investigation*. 2016;126(6):2021-2030. doi:10.1172/JCI84419

32. Sood S, Szkop KJ, Nakhuda A, et al. iGEMS: An integrated model for identification of alternative exon usage events. *Nucleic Acids Res*. 2016;44(11):1-14. doi:10.1093/nar/gkw263

33. Sherman BT, Hao M, Qiu J, et al. DAVID: a web server for functional enrichment analysis and functional annotation of gene lists (2021 update). *Nucleic Acids Res*. Published online March 23, 2022. doi:10.1093/nar/gkac194

34. Day A, Dong J, Funari VA, et al. Disease gene characterization through large-scale co-expression analysis. *PLoS One*. 2009;4(12). doi:10.1371/journal.pone.0008491

35. Song WM, Zhang B. Multiscale Embedded Gene Co-expression Network Analysis. *PLoS Comput Biol*. 2015;11(11). doi:10.1371/journal.pcbi.1004574

36. Ponting CP, Haerty W. Genome-Wide Analysis of Human Long Noncoding RNAs: A Provocative Review. Published online 2022. doi:10.1146/annurev-genom-112921

37. Cabili MN, Dunagin MC, McClanahan PD, et al. Localization and abundance analysis of human lncRNAs at single-cell and single-molecule resolution. *Genome Biol*. 2015;16(1). doi:10.1186/s13059-015-0586-4

38. LOPEZ P, RADAELLI R, TAAFFE DR, et al. Resistance Training Load Effects on Muscle Hypertrophy and Strength Gain: Systematic Review and Network Meta-analysis. *Med Sci Sports Exerc*. 2021;53(6):1206-1216. doi:10.1249/MSS.0000000000002585

39. Morton RW, Oikawa SY, Wavell CG, et al. Neither load nor systemic hormones determine resistance training-mediated hypertrophy or strength gains in resistance-trained young men. *J Appl Physiol*. 2016;121(1):129-138. doi:10.1152/japplphysiol.00154.2016

40. Morton RW. *Resistance Exercise-Induced Muscle Hypertrophy*. McMaster University; 2019.

41. Phillips BE, Kelly BM, Lilja M, et al. A practical and time-efficient high-intensity interval training program modifies cardio-metabolic risk factors in adults with risk factors for type II diabetes. *Front Endocrinol (Lausanne)*. 2017;8(SEP):1-11. doi:10.3389/fendo.2017.00229

42. Mitchell CJ, Churchward-Venne TA, Parise G, et al. Acute post-exercise myofibrillar protein synthesis is not correlated with resistance training-induced muscle hypertrophy in young men. *PLoS One*. 2014;9(2):1-7. doi:10.1371/journal.pone.0089431

43. Powers C, Fan B, Borrud LG, Looker AC, Shepherd JA. Long-term precision of dual-energy X-ray absorptiometry body composition measurements and association with their covariates. *J Clin Densitom*. 2015;18(1):76-85. doi:10.1016/J.JOCD.2013.09.010

44. Barlow MJ, Oldroyd B, Smith D, et al. Precision Error in Dual-Energy X-Ray Absorptiometry Body Composition Measurements in Elite Male Rugby League Players. *J Clin Densitom*. 2015;18(4):546-550. doi:10.1016/J.JOCD.2015.04.008

45. LeBlanc AD, Schneider VS, Evans HJ, Pientok C, Rowe R, Spector E. Regional changes in muscle mass following 17 weeks of bed rest. *https://doi.org/101152/jappl19927352172*. 1992;73(5):2172-2178. doi:10.1152/JAPPL.1992.73.5.2172

46. Sood S, Szkop KJ, Nakhuda A, et al. iGEMS: An integrated model for identification of alternative exon usage events. *Nucleic Acids Res*. 2016;44(11):1-14. doi:10.1093/nar/gkw263

47. Bengtsson H, Simpson K, Bullard J, Hansen K. aroma.affymetrix: A generic framework in R for analyzing small to very large Affymetrix data sets in bounded memory. *Department of Statistics, University of California, Berkeley*. 2008;745:1-9.

48. Harrow J, Frankish A, Gonzalez JM, et al. GENCODE: The reference human genome annotation for the ENCODE project. *Genome Res*. 2012;22(9):1760-1774. doi:10.1101/gr.135350.111

49. Frankish A, Carbonell-Sala S, Diekhans M, et al. GENCODE: reference annotation for the human and mouse genomes in 2023. *Nucleic Acids Res*. 2023;51(D1):D942-D949. doi:10.1093/nar/gkac1071

50. Dobin A, Davis CA, Schlesinger F, et al. STAR: ultrafast universal RNA-seq aligner. *Bioinformatics*. 2013;29(1):15-21. doi:10.1093/BIOINFORMATICS/BTS635

51. Gautier L, Cope L, Bolstad BM, Irizarry RA. Affy - Analysis of Affymetrix GeneChip data at the probe level. *Bioinformatics*. 2004;20(3):307-315. doi:10.1093/bioinformatics/btg405

52. Welsh EA, Eschrich SA, Berglund AE, Fenstermacher DA. Iterative rank-order normalization of gene expression microarray data. *BMC Bioinformatics*. 2013;14. doi:10.1186/1471-2105-14-153

53. Tusher VG, Tibshirani R, Chu G. Significance analysis of microarrays applied to the ionizing radiation response. *Proc Natl Acad Sci U S A*. 2001;98(9):5116-5121. doi:10.1073/PNAS.091062498

54. Shuken SR, McNerney MW. Costs and Benefits of Popular P-Value Correction Methods in Three Models of Quantitative Omic Experiments. *Anal Chem*. 2023;95(5):2732-2740. doi:10.1021/acs.analchem.2c03719

55. Cinar O, Viechtbauer W. The **poolr** Package for Combining Independent and Dependent <math> <mrow> <mi>p</mi> </mrow> </math> Values. *J Stat Softw*. 2022;101(1). doi:10.18637/jss.v101.i01

56. Benjaminit Y, Hochberg Y. Controlling the False Discovery Rate: a Practical and Powerful Approach to Multiple Testing. *J R Statist Soc B*. 1995;57(1):289-300. Accessed January 2, 2022. https://about.jstor.org/terms

57. K.S Pollard, S. Dudoit, M.J. van der Laan. *Multiple Testing Procedures: R Multtest Package and Applications to Genomics, in Bioinformatics and Computational Biology Solutions Using R and Bioconductor*. Springer; 2005.

58. Lai Y, Ramírez-Pardo I, Isern J, et al. Multimodal cell atlas of the ageing human skeletal muscle. *Nature 2024*. Published online April 22, 2024:1-11. doi:10.1038/s41586-024-07348-6

59. Schiaffino S, Rossi AC, Smerdu V, Leinwand LA, Reggiani C. Developmental myosins: expression patterns and functional significance. *Skelet Muscle*. 2015;5(1):22. doi:10.1186/s13395-015-0046-6

60. Talbot J, Maves L. Skeletal muscle fiber type: using insights from muscle developmental biology to dissect targets for susceptibility and resistance to muscle disease. *WIREs Developmental Biology*. 2016;5(4):518-534. doi:10.1002/wdev.230

61. Snijders T, Nederveen JP, McKay BR, et al. Satellite cells in human skeletal muscle plasticity. *Front Physiol*. 2015;6. doi:10.3389/fphys.2015.00283

62. Ritso M, Tung LW, Rossi FMV. Emerging skeletal muscle stromal cell diversity: Functional divergence in fibro/adipogenic progenitor and mural cell populations. *Exp Cell Res*. 2022;410(1). doi:10.1016/J.YEXCR.2021.112947

63. Malm C, Nyberg P, Engström M, et al. Immunological changes in human skeletal muscle and blood after eccentric exercise and multiple biopsies. *J Physiol*. 2000;529(1):243-262. doi:10.1111/j.1469-7793.2000.00243.x

64. Xia C, Babcock HP, Moffitt JR, Zhuang X. Multiplexed detection of RNA using MERFISH and branched DNA amplification. *Sci Rep*. 2019;9(1). doi:10.1038/s41598-019-43943-8

65. Moffitt JR, Bambah-Mukku D, Eichhorn SW, et al. Molecular, spatial, and functional single-cell profiling of the hypothalamic preoptic region. *Science (1979)*. 2018;362(6416). doi:10.1126/science.aau5324

66. Timmons JA, Szkop KJ, Gallagher IJ. Multiple sources of bias confound functional enrichment analysis of global -omics data. *Genome Biol*. 2015;16(1):15-17. doi:10.1186/s13059-015-0761-7

67. Merico D, Isserlin R, Stueker O, Emili A, Bader GD. Enrichment map: A network-based method for gene-set enrichment visualization and interpretation. *PLoS One*. 2010;5(11). doi:10.1371/journal.pone.0013984

68. Xu S, Hu E, Cai Y, et al. Using clusterProfiler to characterize multiomics data. *Nat Protoc*. Published online 2024. doi:10.1038/s41596-024-01020-z

69. Timmons JA, Larsson O, Jansson E, et al. Human muscle gene expression responses to endurance training provide a novel perspective on Duchenne muscular dystrophy. *FASEB Journal*. 2005;19(7):750-760. doi:10.1096/fj.04-1980com

70. Timmons JA, Jansson E, Fischer H, et al. Modulation of extracellular matrix genes reflects the magnitude of physiological adaptation to aerobic exercise training in humans. *BMC Biol*. 2005;3:1-10. doi:10.1186/1741-7007-3-19

71. Scott LJ, Erdos MR, Huyghe JR, et al. The genetic regulatory signature of type 2 diabetes in human skeletal muscle. *Nat Commun*. 2016;7. doi:10.1038/ncomms11764

72. Kulkarni AS, Peck BD, Walton RG, et al. Metformin alters skeletal muscle transcriptome adaptations to resistance training in older adults. *Aging*. 2020;12(20):19852-19866. doi:10.18632/aging.104096

73. Zollinger DR, Lingle SE, Sorg K, Beechem JM, Merritt CR. GeoMx^{TM} RNA Assay: High Multiplex, Digital, Spatial Analysis of RNA in FFPE Tissue. *Methods Mol Biol*. 2020;2148:331-345. doi:10.1007/978-1-0716-0623-0_21

74. Chang MW, Yang JH, Tsitsipatis D, et al. Enhanced myogenesis through lncFAM-mediated recruitment of HNRNPL to the MYBPC2 promoter. *Nucleic Acids Res*. 2022;50(22):13026-13044. doi:10.1093/nar/gkac1174

75. Li A, Nelson SR, Rahmanseresht S, et al. Skeletal MyBP-C isoforms tune the molecular contractility of divergent skeletal muscle systems. *Proc Natl Acad Sci U S A*. 2019;116(43):21882-21892. doi:10.1073/PNAS.1910549116/SUPPL_FILE/PNAS.1910549116.SAPP.PDF

76. Gurnett CA, Desruisseau DM, McCall K, et al. Myosin binding protein C1: a novel gene for autosomal dominant distal arthrogryposis type 1. *Hum Mol Genet*. 2010;19(7):1165-1173. doi:10.1093/HMG/DDP587

77. Timmons JA, Knudsen S, Rankinen T, et al. Using molecular classification to predict gains in maximal aerobic capacity following endurance exercise training in humans. *J Appl Physiol*. 2010;108(6):1487-1496. doi:10.1152/japplphysiol.01295.2009

78. Dill TL, Carroll A, Pinheiro A, Gao J, Naya FJ. The long noncoding RNA Meg3 regulates myoblast plasticity and muscle regeneration through epithelial-mesenchymal transition. *Development (Cambridge)*. 2021;148(2). doi:10.1242/dev.194027

79. Dong K, Shen J, He X, et al. CARMN Is an Evolutionarily Conserved Smooth Muscle Cell-Specific LncRNA That Maintains Contractile Phenotype by Binding Myocardin. *Circulation*. 2021;144(23):1856-1875. doi:10.1161/CIRCULATIONAHA.121.055949

80. Shepro D, Morel NML. Pericyte physiology. *The FASEB Journal*. 1993;7(11):1031-1038. doi:10.1096/fasebj.7.11.8370472

81. de Goede OM, Nachun DC, Ferraro NM, et al. Population-scale tissue transcriptomics maps long non-coding RNAs to complex disease. *Cell*. 2021;184(10):2633-2648.e19. doi:10.1016/j.cell.2021.03.050

82. Lessard L, Liu M, Marzese DM, et al. The CASC15 Long Intergenic Noncoding RNA Locus Is Involved in Melanoma Progression and Phenotype Switching. *Journal of Investigative Dermatology*. 2015;135(10):2464-2474. doi:10.1038/jid.2015.200

83. Wang C, Morley SC, Donermeyer D, et al. Actin-bundling protein L-plastin regulates T cell activation. *J Immunol*. 2010;185(12):7487-7497. doi:10.4049/JIMMUNOL.1001424

84. Wattez JS, Eury E, Hazen BC, et al. Loss of skeletal muscle estrogen-related receptors leads to severe exercise intolerance. *Mol Metab*. 2023;68:101670. doi:10.1016/j.molmet.2023.101670

85. Badin PM, Vila IK, Sopariwala DH, et al. Exercise-like effects by Estrogen-related receptor-gamma in muscle do not prevent insulin resistance in db/db mice. *Sci Rep*. 2016;6(1):26442. doi:10.1038/srep26442

86. Narkar VA, Fan W, Downes M, et al. Exercise and PGC-1α-Independent Synchronization of Type I Muscle Metabolism and Vasculature by ERRγ. *Cell Metab*. 2011;13(3):283-293. doi:10.1016/j.cmet.2011.01.019

87. Wang L, Mascher H, Psilander N, Blomstrand E, Sahlin K. Resistance exercise enhances the molecular signaling of mitochondrial biogenesis induced by endurance exercise in human skeletal muscle. *J Appl Physiol*. 2011;111(5):1335-1344. doi:10.1152/japplphysiol.00086.2011

88. Roberts MD, Romero MA, Mobley CB, et al. Skeletal muscle mitochondrial volume and myozenin-1 protein differences exist between high versus low anabolic responders to resistance training. *PeerJ*. 2018;2018(7). doi:10.7717/peerj.5338

89. Bryce S, Stolzer M, Crosby D, Yang R, Durand D, Lee TH. Human atlastin-3 is a constitutive ER membrane fusion catalyst. *J Cell Biol*. 2023;222(7). doi:10.1083/JCB.202211021

90. Mohammadi S, Jafari Khamirani H, Baneshi M, et al. A novel nonsense variant in the ATL3 gene is associated with disturbed pain sensitivity, numbness of distal limbs and muscle weakness. *Ann Hum Genet*. 2023;87(4):147-157. doi:10.1111/AHG.12501

91. Cheetham SW, Faulkner GJ, Dinger ME. Overcoming challenges and dogmas to understand the functions of pseudogenes. *Nat Rev Genet*. 2020;21(3):191-201. doi:10.1038/s41576-019-0196-1

92. Jubran J, Hekselman I, Novack L, Yeger-Lotem E. Dosage-sensitive molecular mechanisms are associated with the tissue-specificity of traits and diseases. *Comput Struct Biotechnol J*. 2020;18:4024-4032. doi:10.1016/j.csbj.2020.10.030

93. Sartori R, Romanello V, Sandri M. Mechanisms of muscle atrophy and hypertrophy: implications in health and disease. *Nat Commun*. 2021;12(1):330. doi:10.1038/s41467-020-20123-1

94. McIntosh MC, Anglin DA, Robinson AT, Beck DT, Roberts MD. Making the case for resistance training in improving vascular function and skeletal muscle capillarization. *Front Physiol*. 2024;15. doi:10.3389/fphys.2024.1338507

95. Wohlwend M, Laurila PP, Williams K, et al. *The Exercise-Induced Long Noncoding RNA CYTOR Promotes Fast-Twitch Myogenesis in Aging*. Vol 13.; 2021. https://www.science.org

96. Tumasian RA, Harish A, Kundu G, et al. Skeletal muscle transcriptome in healthy aging. *Nat Commun*. 2021;12(1). doi:10.1038/s41467-021-22168-2

97. Neppl RL, Wu CL, Walsh K. lncRNA Chronos is an aging-induced inhibitor of muscle hypertrophy. *Journal of Cell Biology*. 2017;216(11):3497-3507. doi:10.1083/jcb.201612100

98. Zheng Y, Liu T, Li Q, Li J. Integrated analysis of long non-coding RNAs (lncRNAs) and mRNA expression profiles identifies lncRNA PRKG1-AS1 playing important roles in skeletal muscle aging. *Aging*. 2021;13(11):15044-15060. doi:10.18632/aging.203067

99. Liang R, Shen X, Wang F, et al. H19X-encoded miR-322(424)/miR-503 regulates muscle mass by targeting translation initiation factors. *J Cachexia Sarcopenia Muscle*. 2021;12(6):2174-2186. doi:10.1002/jcsm.12827

100. Zhang Y, Li Y, Hu Q, et al. The lncRNA H19 alleviates muscular dystrophy by stabilizing dystrophin. *Nat Cell Biol*. 2020;22(11):1332-1345. doi:10.1038/S41556-020-00595-5

101. Ervasti JM. Dystrophin, its interactions with other proteins, and implications for muscular dystrophy. *Biochimica et Biophysica Acta (BBA) - Molecular Basis of Disease*. 2007;1772(2):108-117. doi:10.1016/J.BBADIS.2006.05.010

102. Ziemkiewicz N, Hilliard G, Pullen NA, Garg K. The role of innate and adaptive immune cells in skeletal muscle regeneration. *Int J Mol Sci*. 2021;22(6). doi:10.3390/ijms22063265

103. Langston PK, Sun Y, Ryback BA, et al. Regulatory T cells shield muscle mitochondria from interferon-γ-mediated damage to promote the beneficial effects of exercise. Published online 2023. https://www.science.org

104. Dumont NA, Bentzinger CF, Sincennes M, Rudnicki MA. Satellite Cells and Skeletal Muscle Regeneration. In: *Comprehensive Physiology*. Wiley; 2015:1027-1059. doi:10.1002/cphy.c140068

105. Sun Q, Hao Q, Prasanth K V. Nuclear Long Noncoding RNAs: Key Regulators of Gene Expression. *Trends in Genetics*. 2018;34(2):142-157. doi:10.1016/j.tig.2017.11.005

106. Ackermann MA, Kontrogianni-Konstantopoulos A. Myosin Binding Protein-C: A Regulator of Actomyosin Interaction in Striated Muscle. *J Biomed Biotechnol*. 2011;2011:1-9. doi:10.1155/2011/636403

107. Mayeur GL, Fraser CS, Peiretti F, Block KL, Hershey JWB. Characterization of eIF3k. *Eur J Biochem*. 2003;270(20):4133-4139. doi:10.1046/j.1432-1033.2003.03807.x

108. Stouthamer AH. A theoretical study on the amount of ATP required for synthesis of microbial cell material. *Antonie Van Leeuwenhoek*. 1973;39(1):545-565. doi:10.1007/BF02578899

109. Zhou Y, Zhang X, Klibanski A. MEG3 noncoding RNA: a tumor suppressor. *J Mol Endocrinol*. 2012;48(3):R45-R53. doi:10.1530/JME-12-0008

110. Miyoshi N, Wagatsuma H, Wakana S, et al. Identification of an imprinted gene, *Meg3* / *Gtl2* and its human homologue *MEG3* , first mapped on mouse distal chromosome 12 and human chromosome 14q. *Genes to Cells*. 2000;5(3):211-220. doi:10.1046/j.1365-2443.2000.00320.x

111. Zhao J, Ohsumi TK, Kung JT, et al. Genome-wide Identification of Polycomb-Associated RNAs by RIP-seq. *Mol Cell*. 2010;40(6):939-953. doi:10.1016/j.molcel.2010.12.011

112. Waddell JN, Zhang P, Wen Y, et al. Dlk1 Is Necessary for Proper Skeletal Muscle Development and Regeneration. *PLoS One*. 2010;5(11):e15055. doi:10.1371/journal.pone.0015055

113. Andersen DC, Petersson SJ, Jørgensen LH, et al. Characterization of DLK1+ Cells Emerging During Skeletal Muscle Remodeling in Response to Myositis, Myopathies, and Acute Injury. *Stem Cells*. 2009;27(4):898-908. doi:10.1634/stemcells.2008-0826

114. Davis E, Jensen CH, Schroder HD, et al. Ectopic Expression of DLK1 Protein in Skeletal Muscle of Padumnal Heterozygotes Causes the Callipyge Phenotype. *Current Biology*. 2004;14(20):1858-1862. doi:10.1016/j.cub.2004.09.079

115. Cohen P. THE STRUCTURE AND REGULATION OF PROTEIN PHOSPHATASES. *Annu Rev Biochem*. 1989;58(1):453-508. doi:10.1146/annurev.bi.58.070189.002321

116. Seila AC, Calabrese JM, Levine SS, et al. Divergent transcription from active promoters. *Science*. 2008;322(5909):1849-1851. doi:10.1126/science.1162253

117. Luo S, Lu JY, Liu L, et al. Divergent lncRNAs Regulate Gene Expression and Lineage Differentiation in Pluripotent Cells. *Cell Stem Cell*. 2016;18(5):637-652. doi:10.1016/j.stem.2016.01.024

118. Subhash S, Mishra K, Akhade VS, Kanduri M, Mondal T, Kanduri C. H3K4me2 and WDR5 enriched chromatin interacting long non-coding RNAs maintain transcriptionally competent chromatin at divergent transcriptional units. *Nucleic Acids Res*. 2018;46(18):9384-9400. doi:10.1093/nar/gky635

119. Betz MW, Aussieker T, Kruger CQ, Gorissen SHM, van Loon LJC, Snijders T. Muscle fiber capillarization is associated with various indices of skeletal muscle mass in healthy, older men. *Exp Gerontol*. 2021;143. doi:10.1016/j.exger.2020.111161

120. Thomas ACQ, Brown A, Hatt AA, et al. Short-term aerobic conditioning prior to resistance training augments muscle hypertrophy and satellite cell content in healthy young men and women. *FASEB Journal*. 2022;36(9). doi:10.1096/fj.202200398RR

121. Smart N, Rossdeutsch A, Riley PR. Thymosin β4 and angiogenesis: modes of action and therapeutic potential. *Angiogenesis*. 2007;10(4):229-241. doi:10.1007/s10456-007-9077-x

122. Sasikumar AN, Perez WB, Kinzy TG. The many roles of the eukaryotic elongation factor 1 complex. *WIREs RNA*. 2012;3(4):543-555. doi:10.1002/wrna.1118

123. Glenfield C, McLysaght A. Pseudogenes Provide Evolutionary Evidence for the Competitive Endogenous RNA Hypothesis. *Mol Biol Evol*. Published online September 25, 2018. doi:10.1093/molbev/msy183

124. Hildebrandt W, Schwarzbach H, Pardun A, et al. Age-related differences in skeletal muscle microvascular response to exercise as detected by contrast-enhanced ultrasound (CEUS). *PLoS One*. 2017;12(3):e0172771. doi:10.1371/journal.pone.0172771

125. Phillips BE, Atherton PJ, Varadhan K, et al. The effects of resistance exercise training on macro- and micro-circulatory responses to feeding and skeletal muscle protein anabolism in older men. *J Physiol*. 2015;593(12):2721-2734. doi:10.1113/JP270343

126. Kotzin JJ, Spencer SP, McCright SJ, et al. The long non-coding RNA Morrbid regulates Bim and short-lived myeloid cell lifespan. *Nature*. 2016;537(7619):239-243. doi:10.1038/nature19346

127. Lee U, Stuelsatz P, Karaz S, et al. A Tead1-Apelin axis directs paracrine communication from myogenic to endothelial cells in skeletal muscle. *iScience*. 2022;25(7). doi:10.1016/J.ISCI.2022.104589

128. Coletta G, Phillips SM. An elusive consensus definition of sarcopenia impedes research and clinical treatment: A narrative review. *Ageing Res Rev*. 2023;86. doi:10.1016/J.ARR.2023.101883

129. Heberle H, Meirelles VG, da Silva FR, Telles GP, Minghim R. InteractiVenn: a web-based tool for the analysis of sets through Venn diagrams. *BMC Bioinformatics*. 2015;16(1). doi:10.1186/S12859-015-0611-3

130. Yue Y, Yue Y, Fan Z, et al. The long noncoding RNA lnc-H19 is important for endurance exercise by maintaining slow muscle fiber types. *Journal of Biological Chemistry*. 2023;299(11):105281. doi:10.1016/j.jbc.2023.105281

FIGURES:

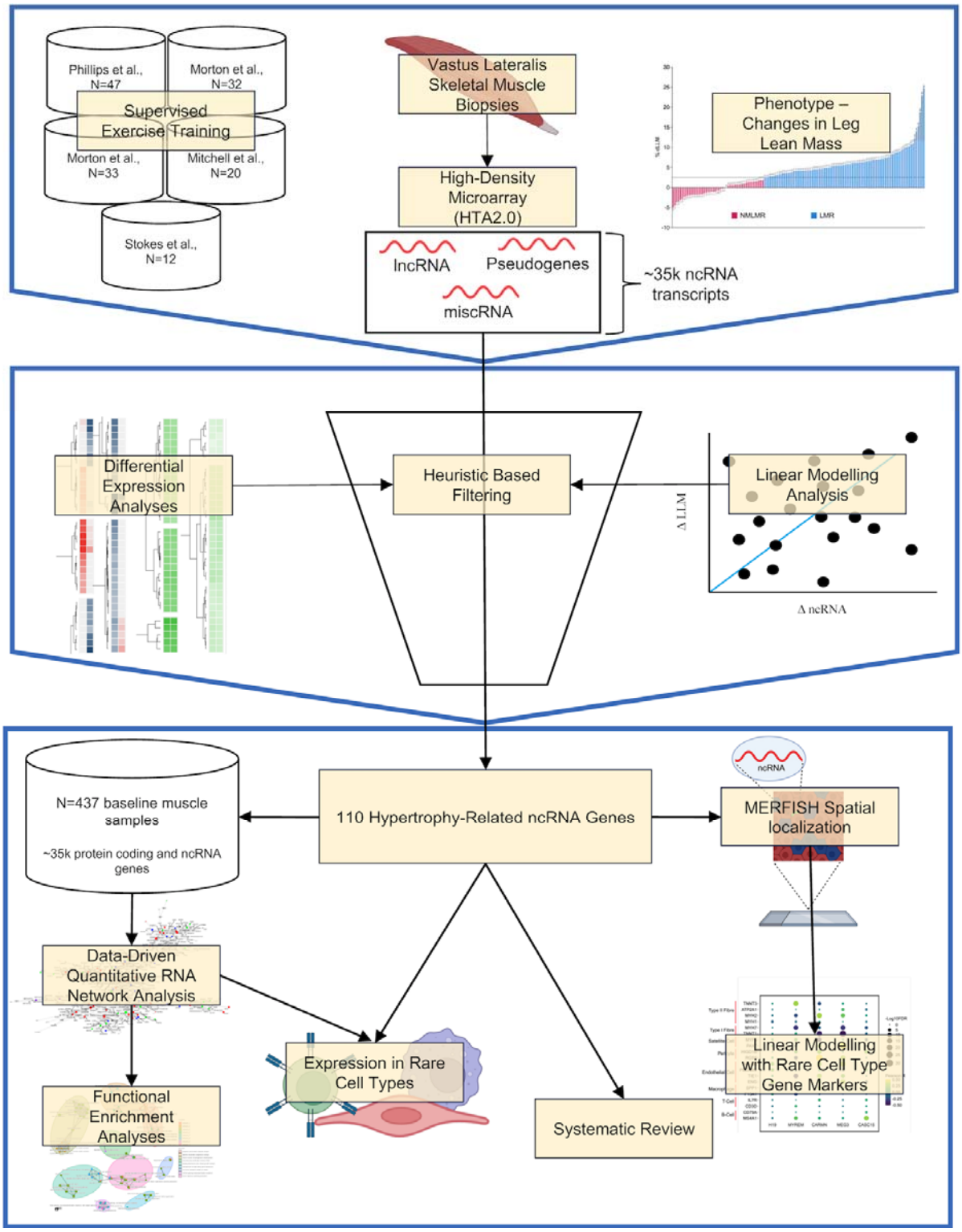

Figure 1. Overview of the analysis pipeline. We used 144 participants from five supervised muscle-loading studies. We measured skeletal muscle hypertrophy (using DXA and MRI), and 88 individuals exhibited a change in skeletal muscle hypertrophy beyond the technical variation

of our measurement instruments. RNA was extracted from skeletal muscle samples pre- and post-training, and we quantified ncRNA transcriptome (miscRNA, lncRNA and pseudogenes) using the Human Transcriptome Array 2.0. Using differential expression analyses, linear modelling analysis, and heuristic-based filtering, we established 110 ncRNA genes are related to skeletal muscle hypertrophy. We used RNA network modelling analysis in baseline bulk skeletal muscle samples (n=437) of protein-coding and ncRNA genes. We used a novel transcript spatial localisation method to help facilitate the discovery of functional pathways and cell-type specific associations that several key ncRNA genes belong to.

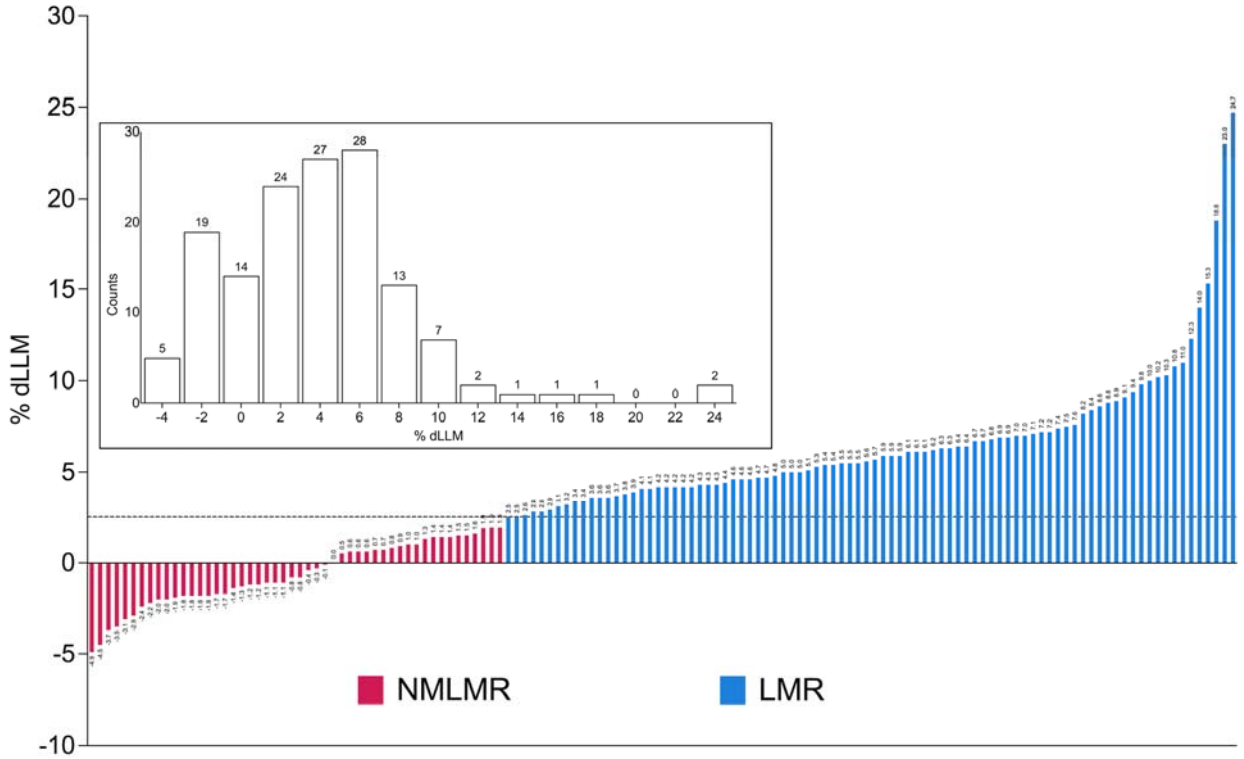

Figure 2. Phenotypic overview of included studies. Waterfall plot showing the percent change in leg lean mass (% dLLM) for 138 participants used for differential expression analyses. The dotted line (2.5% dLLM) depicts the threshold for the precision error of the DXA and MRI. Individuals who exhibited a ≥ 2.5% dLLM (or quadriceps muscle volume for MRI) were allocated to the group: "Lean Mass Responders" (LMR; n=88), whereas individuals who showed < 2.0% dLLM were assigned to the group called "No Measurable Lean Mass Response" (NMLMR; n=50). Each bar corresponds to one individual, and the number above each bar corresponds to the numerical value for dLLM%. Box Inset: Histogram depicts the number of individuals (144) falling into each %dLLM bin, and counts above each bar correspond to the number of individuals in that particular %dLLM bin. For a detailed overview of participant characteristics, please refer to Table S1.

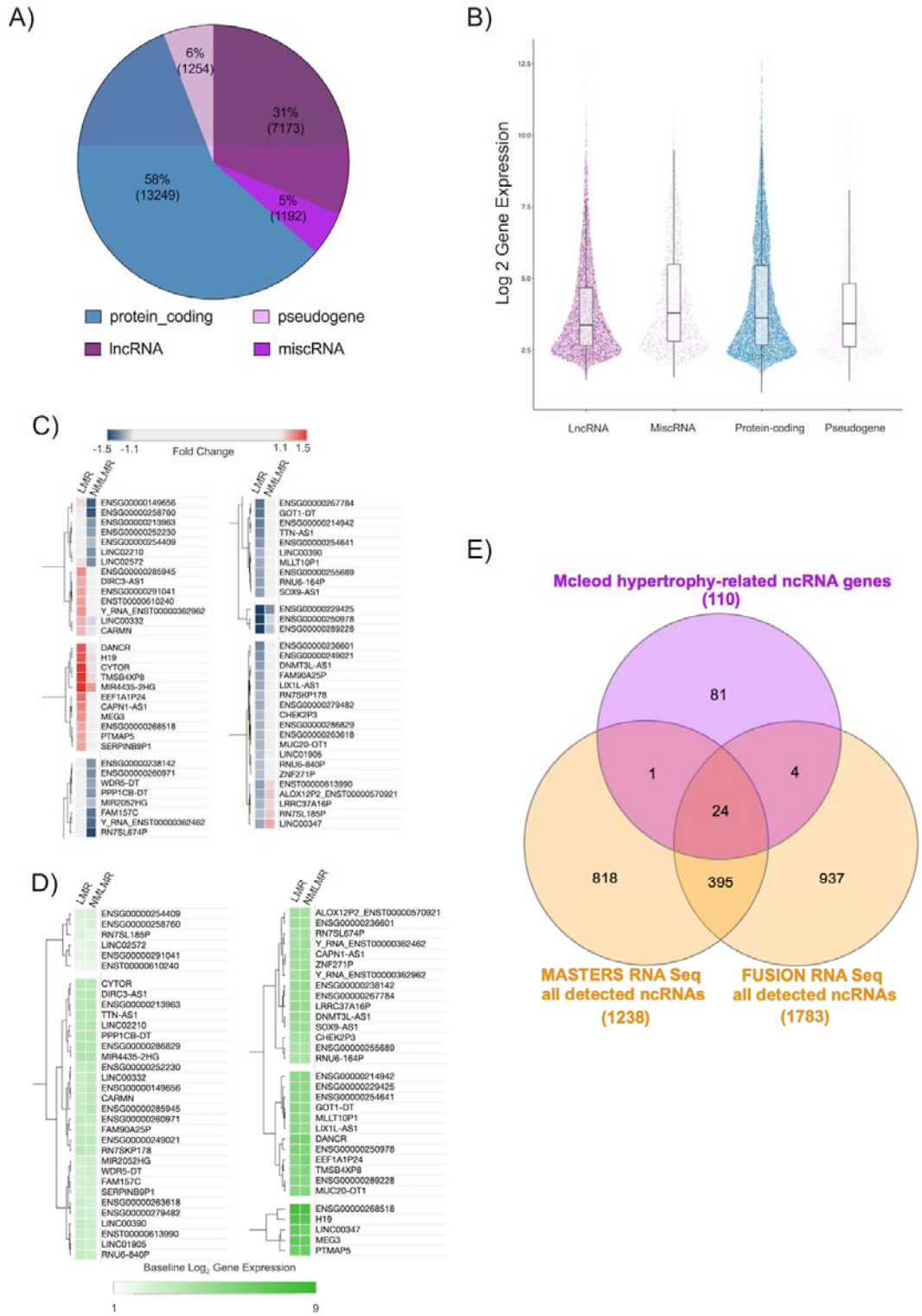

Figure 3. RNA molecules quantified on high-density arrays and establishing a 110 ncRNA gene signature associated with skeletal muscle hypertrophy. A) Quantitative overview of the number of genes (2 SD filter applied to protein-coding genes and 1 SD filter to ncRNA genes) belonging to each class of RNA. B) The distribution of the abundance (log 2 signal) of each

RNA class is visualised using the median (horizontal line within the box), upper and lower interquartile ranges (upper and lower edges of the box), upper and lower whiskers (1.5 x interquartile range), and the points correspond to an individual gene. C) Heat plot that denotes fold changes for 65 ncRNA genes were differentially expressed and uniquely regulated in a manner that was distinct across the LMR group (50 genes) and the NMLMR group (15 genes). (D) The heat plot denotes the log2 baseline gene expression for the 65 uniquely regulated ncRNA genes. The heat plots (C, D) were created using Morpheus (https://clue.io/Morpheus), and genes were hierarchically clustered using Euclidean distance (linkage method: complete). E) 110 hypertrophy-related ncRNA genes were contrasted to all consistently detected ncRNA genes from two short-read RNA sequencing data sets profiling skeletal muscle (MASTERS ≈34 million reads, n = 136 [72]; FUSION ≈60 million reads, n =278 [71] using a Venn diagram tool (https://www.interactivenn.net/; [129]).

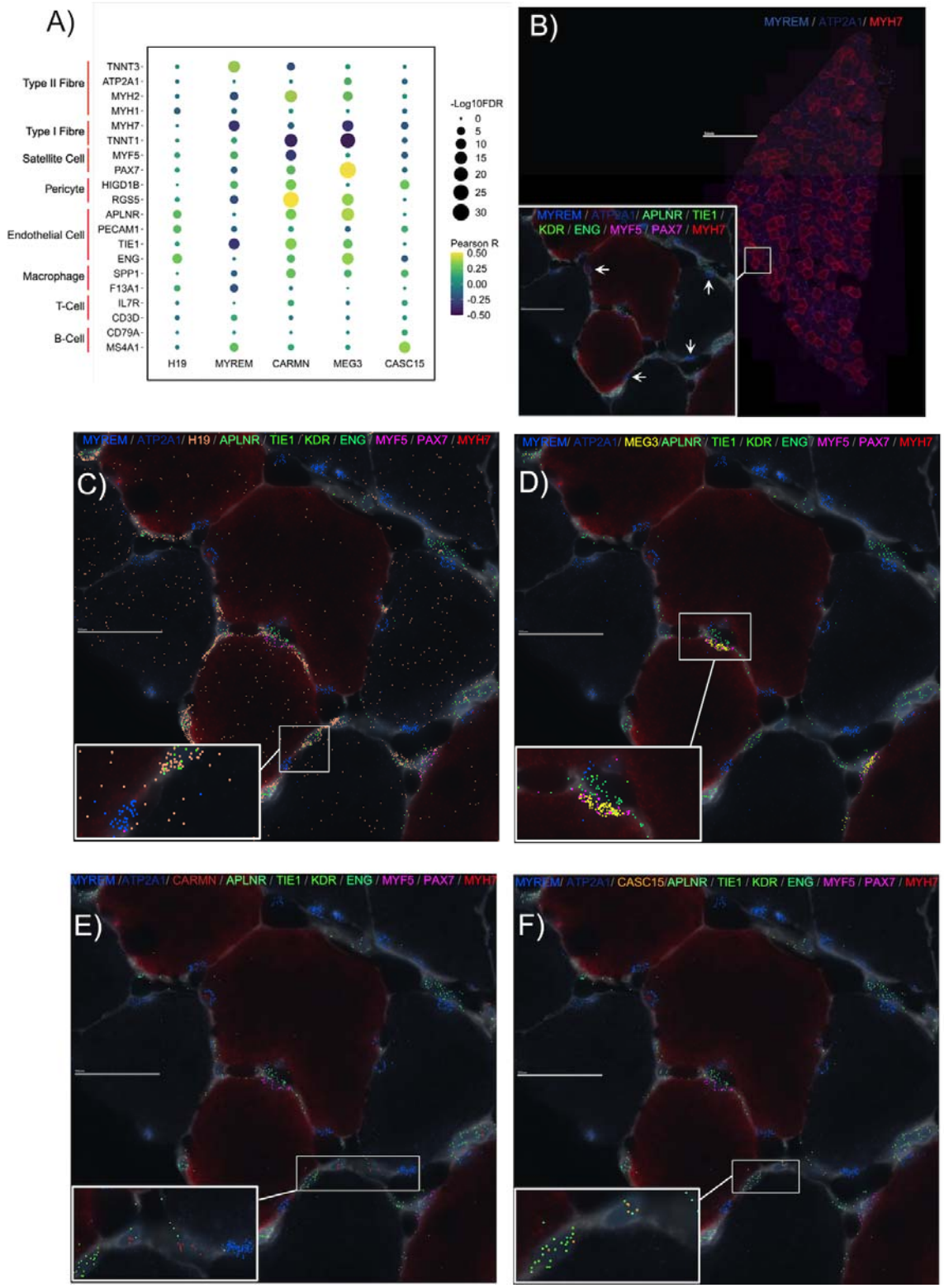

Figure 4. Spatially resolving several hypertrophy-related ncRNA genes in human skeletal muscle *in vivo*. A) Dot plot depicting the association between the expression of hypertrophy-related ncRNA genes - that were used for MERFISH - and gene markers for skeletal muscle fibre

types and rare mononuclear cell types, using bulk transcriptomic data (n=437). The colour of the dot corresponds to the Pearson correlation coefficient, and the size of the dot is proportional to the –Log10 FDR. B) High-level image of type I (*MYH7*) and type II (*ATP2A1*) FISH probes on a human skeletal muscle cross-section. Box inset shows magnified region of skeletal muscle cross-section with MERFISH probes for *MYREM*, as well as MERFISH probes for endothelial cell protein-coding gene markers (*APLNR*, *TIE1*, *KDR*, *ENG*) and satellite cell protein-coding gene markers (*MYF5*, *PAX7*). The spatial distribution of C) *H19*, D) *MEG3*, E) *CARMN*, and F) *CASC15*, all with the same magnification, location, and protein-coding MERFISH probes as box inset in B).

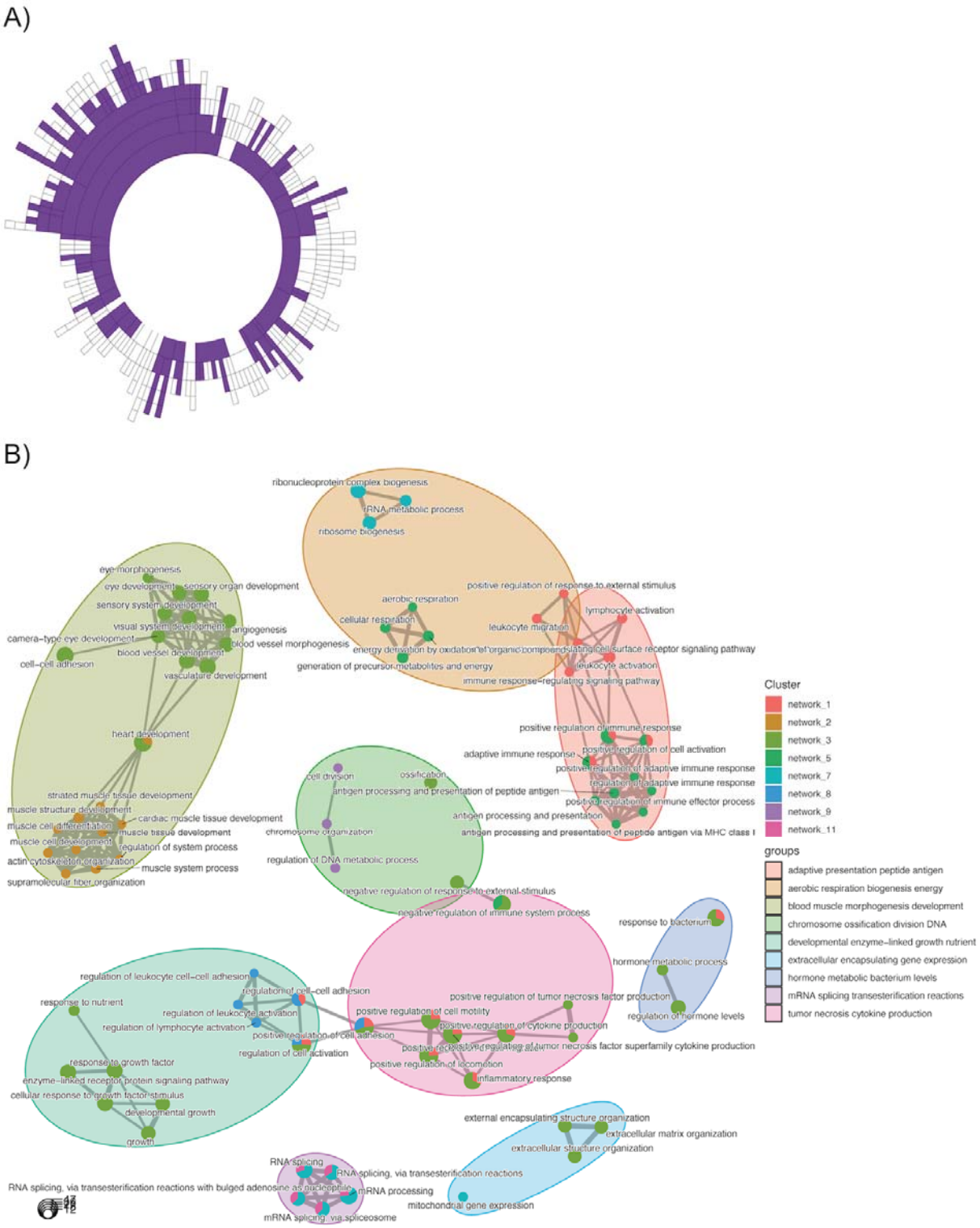

Figure 5. Discovery of interacting functional pathways that contain hypertrophy-related ncRNA genes. A) Sunburst plot denoting the hierarchical organisation of ncRNA containing co-expression network modules constructed from 437 resting skeletal muscle biopsy samples (< 50 years old), using MEGENA [35]. Each concentric ring corresponds to a cluster of co-expressed

genes, with the size of the ring being proportional to the number of genes. Purple concentric rings are modules that contain at least one of the 110 hypertrophy-related ncRNA genes. B) Using the compareCluster function[67,68] in the ClusterProfiler R package and the GOTERM_BP_ALL from DAVID as the ontology database, and the ~13.4K protein coding genes expressed in muscle, we established the relationships between hypertrophy ncRNA containing modules. A q-value of 1% was utilized as a filter for presentating significant ontologies. Pie-charts illustrate when genes from more than one network contribute to an individual significant ontology catergory, while some ontology catergories extend across distinct grouped functions. Further, each network can contain multiple ontologies which also show overlap within and across groups of functional processes. Finally, there is evidence that interacting groups of functions occur at the level of immune cell types. This analysis demonstrates that the ncRNAs interact at both the pathway and cell interaction level in a coordinated manner.

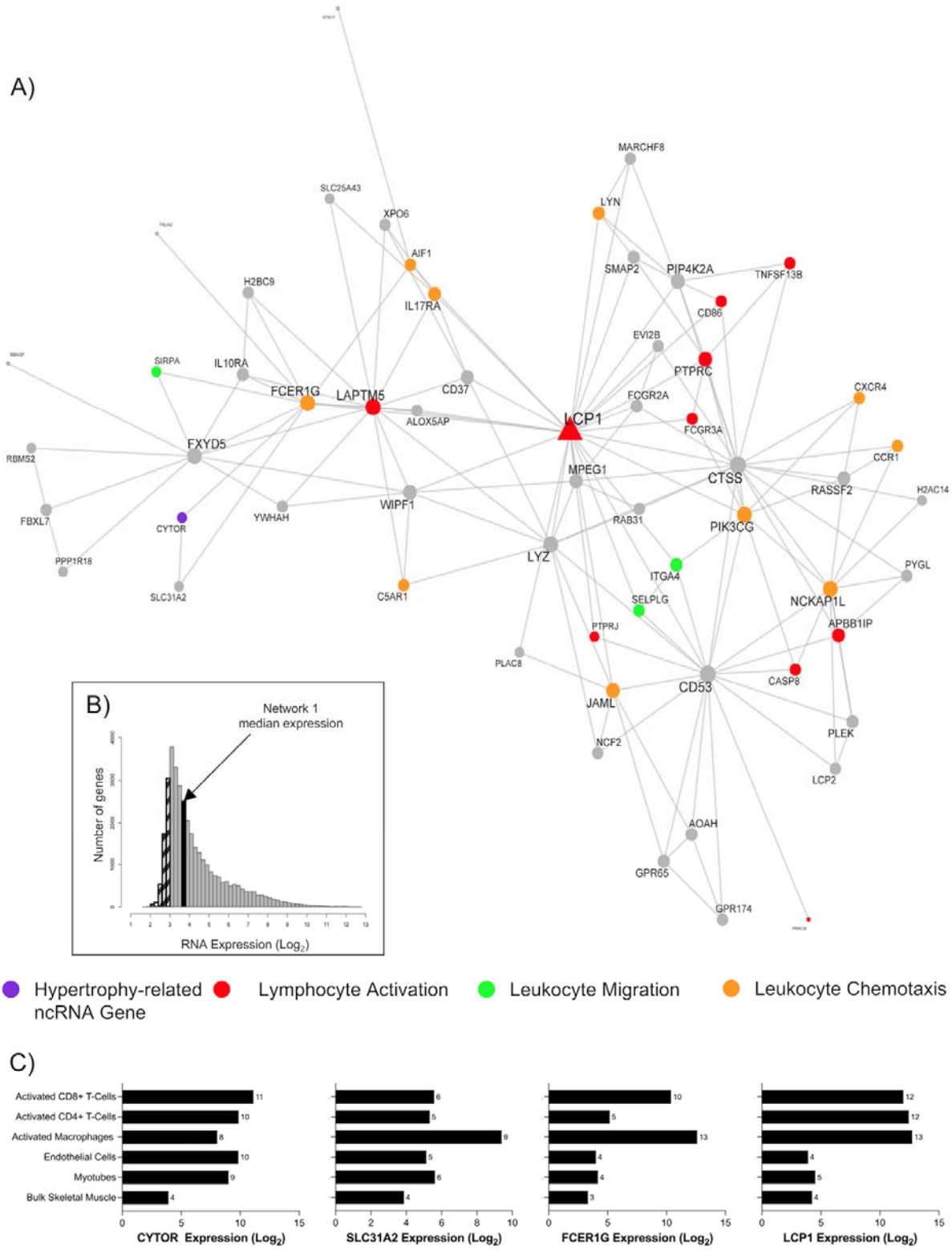

Figure 6. *CYTOR* is the only ncRNA gene co-expressed in network 1 and biologically associated with immune cell-related functions. A) A biologically enriched gene co-expression network (network 1; table 1), which contains the hypertrophy-related ncRNA gene, *CYTOR*

(purple). This network of genes is related to immunological biological processes, such as lymphocyte activation (red), leukocyte migration (green), and leukocyte chemotaxis (orange). Node and label size are proportional to node degree value within each network, and triangle symbols denote genes that are hubs of the cluster of co-expressed genes. B) A frequency plot of the median $\log_2$ expression of 35k genes in resting bulk skeletal muscle. Hatched bars reflect gene signals most likely indistinguishable from background signal [15]. The black bar denotes the median $\log_2$ expression of all 60 genes apart from network 1. C) The log2 expression of several network 1 genes (*CYTOR*, *SLC31A2*, *FCER1G*, *LCP1*) in bulk skeletal muscle, human myotubes, endothelial cells, activated macrophages, CD8+ T cells, and CD4+ T cells.

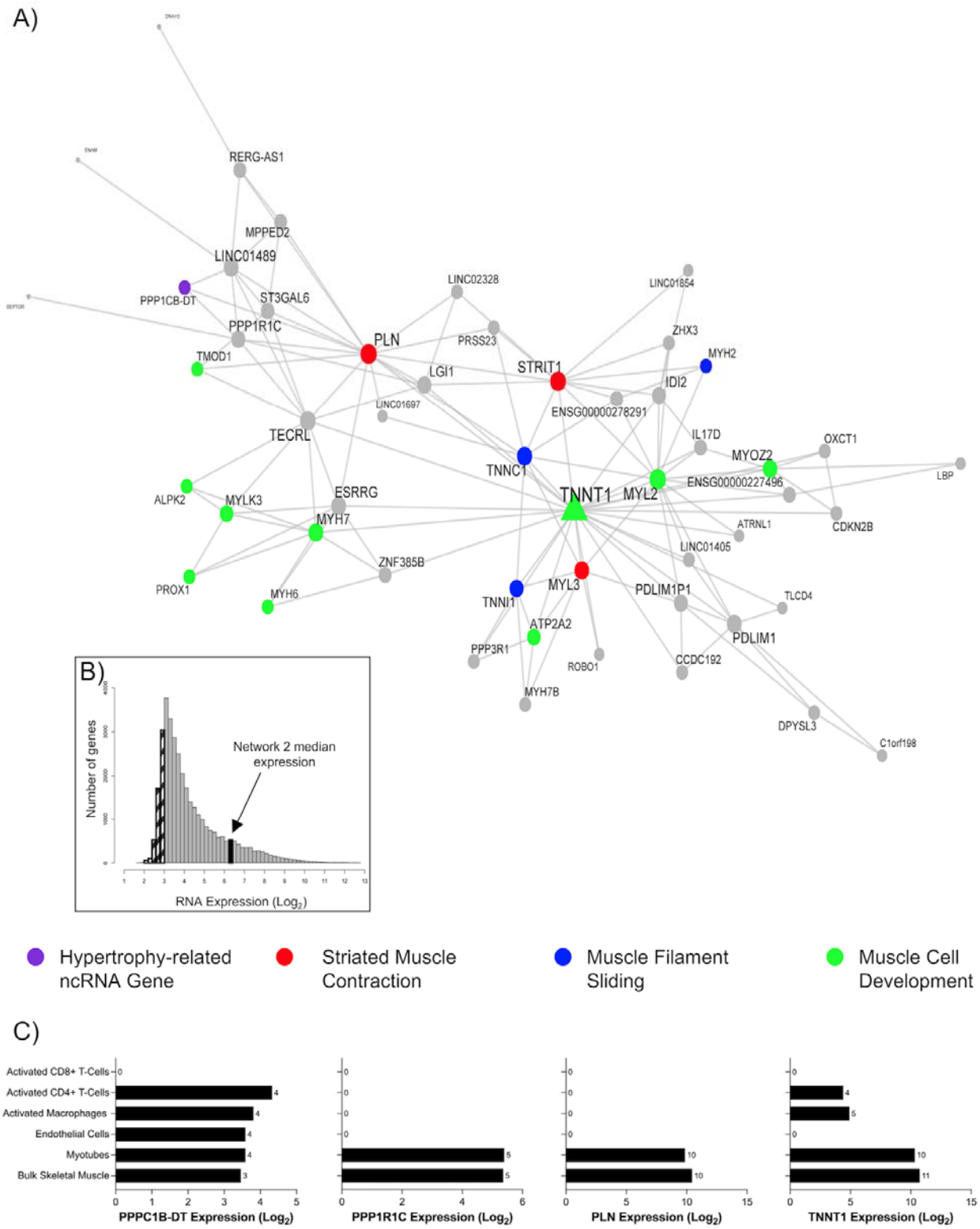

Figure 7 A highly expressed gene co-expression network in skeletal muscle is related to muscle remodelling processes. A) Network 2 is composed of 52 genes and contains the hypertrophy-related ncRNA gene, phosphatase 1 catalytic subunit beta divergent transcript

(*PPP1CB-DT*; purple). This network of genes is related to skeletal muscle remodelling processes, such as striated muscle contraction (red), muscle filament sliding (blue), and muscle cell development (green). Node and label size are proportional to node degree value within each network, and triangle symbols denote genes that are hubs of the cluster of co-expressed genes. B) A frequency plot of the median $\log_2$ expression of 35k genes in resting bulk skeletal muscle. Hatched bars reflect gene signals most likely indistinguishable from background signal [15]. The black bar denotes the median $\log_2$ expression of all 52 genes apart from network 2. C) The log2 expression of several network 2 genes (*PPPC1B-DT*, *PP1R1C*, *PLN*, *TNNT1*) in bulk skeletal muscle, human myotubes, endothelial cells, activated macrophages, CD8+ T cells, and CD4+ T cells.

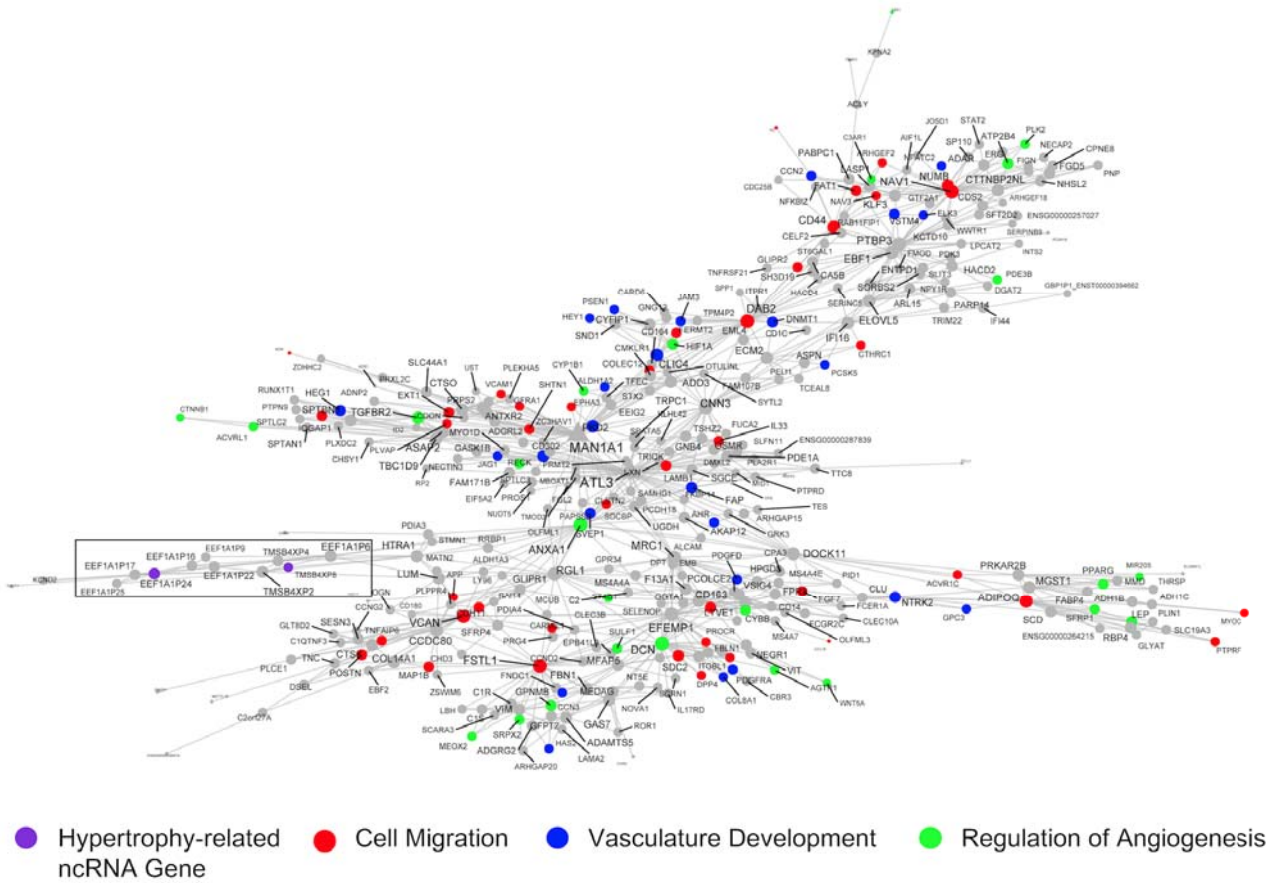

Figure 8. RNA network related to vascular remodelling harbours a pair of pseudogenes related to skeletal muscle hypertrophy. This network is one of the largest gene co-expression RNA networks (370 genes), and a significant proportion of genes are associated with cell migration (red), vasculature development (blue), and regulation of angiogenesis (green). Embedded in this network are a cluster of pseudogenes (*EEF1A1P9*, *EEF1A1P24*, *EEF1A1P17*, *EEF1A1P25*, *EEF1A1P22*, *EEF1A1P16*, *EEF1A1P6*, *TMSB4XP4*, *TMSB4XP2*, *TMSB4XP8;* black box), two of which are hypertrophy-related ncRNA genes (*TMSB4XP8* and *EEF1A1P24*, purple). Node and label size are proportional to node degree value within each network, and triangle symbols denote genes that are hubs of the cluster of co-expressed genes.

TABLES:

Table 1. Summary of biologically relevant significant RNA co-expression modules containing hypertrophy-related ncRNA genes.

Network	Non-coding candidate	Module size	Module biotype composition	Biological processes	Cellular components
1 (Figure 6)	CYTOR	60	98% protein-coding, 2% lncRNA, 0% miscRNA, 0% pseudogene	Lymphocyte activation (FDR = 4.96 x 10^{-7}; FE = 6.62). Leukocyte migration (FDR = 1.05 x 10^{-6}; FE = 10.61). Leukocyte chemotaxis (FDR = 1.56 x 10^{-5}; FE = 13.42).	Plasma membrane part (FDR = 1.53 x 10^{-9}; FE = 3.44). Integral component of plasma membrane (FDR = 3.02 x 10^{-7}; FE = 4.39). Intrinsic component of plasma membrane (FDR = 4.83 x 10^{-7}; FE = 4.18).
2 (Figure 7)	PPP1CB-DT	52	81% protein-coding, 17% lncRNA, 0% miscRNA, 2% pseudogene	Myofibril assembly (FDR = 8.15 x 10^{-8}; FE = 47.52). Cellular component assembly involved in morphogenesis (FDR = 8.15 x 10^{-8}; FE = 30.68). Striated muscle contraction (FDR = 8.15 x 10^{-8}; FE = 22.15).	Myofibril (FDR = 5.84 x 10^{-10}; FE = 19.75). Contractile fiber (FDR = 5.84 x 10^{-10}; FE = 19.02). Sarcomere (FDR = 2.72 x 10^{-9}; FE = 19.86).
3 (Figure 8)	EEF1A1P24, TMSB4XP8	370	95% protein-coding, 2% lncRNA, 0% miscRNA, 4% pseudogene	Cell migration (FDR = 5.05 x 10^{-12}; FE =2.64). Cardiovascular system development (FDR = 2.28 x 10^{-9}; FE =3.11). Vasculature development (FDR = 2.28 x 10^{-9}; FE =3.11).	Extracellular exosome (FDR = 3.96 x 10^{-6}; FE = 1.90). Plasma membrane part (FDR = 3.96 x 10^{-6}; FE = 1.74). Intrinsic component of plasma membrane (FDR = 2.20 x 10^{-5}; FE = 2.02).
4 (Figure S5)	MYREM	105	85% protein-coding, 11% lncRNA, 3% miscRNA, 1% pseudogene	N/S	Mitochondrial inner membrane (FDR = 3.24 x 10^{-5}; FE = 5.99).
5	FAM157C	224	79% protein-coding, 27% lncRNA, 3% miscRNA, 5% pseudogene	Positive regulation of T cell-mediated cytotoxicity (FDR = 2.93 x 10^{-5}; FE =26.14). Antigen processing and presentation of exogenous peptide antigen via MHC class I (FDR = 2.93 x 10^{-5}; FE =23.76). Antigen processing and presentation of endogenous peptide antigen via MHC class I (FDR = 2.93 x 10^{-5}; FE = 32.67).	MHC protein complex (FDR = 1.35 x 10^{-8}; FE = 38.15). Intrinsic component of endoplasmic reticulum membrane (FDR = 3.32 x 10^{-7}; FE = 8.60). An integral component of the lumenal side of the endoplasmic reticulum membrane (FDR = 3.33 x 10^{-5}; FE = 31.20).
6	DNMT3L-AS1, LINC01792, LINC01122, ENSG00000273674, ENSG00000258760	305	43% protein-coding, 45% lncRNA, 9% miscRNA, 3% pseudogene	N/S	Intermediate filament (FDR = 4.77 x 10^{-6}; FE = 14.37). Intermediate filament cytoskeleton (FDR = 1.94 x 10^{-5}; FE = 11.26).
7	LINC02210	385	83% protein-coding, 10% lncRNA, 3% miscRNA, 4% pseudogene	Nucleic acid metabolic process (FDR = 1.48 x 10^{-7}; FE = 1.57). RNA processing (FDR = 1.01 x 10^{-5}; FE = 2.41). RNA metabolic process (FDR = 1.31 x 10^{-5}; FE = 1.53).	Nuclear lumen (FDR = 5.08 x 10^{-11}; FE = 1.68). Nuclear part (FDR = 1.99 x 10^{-10}; FE = 1.61). Intracellular organelle lumen (FDR = 1.99 x 10^{-10}; FE = 1.54).
8	MIR4435-2HG	112	90% protein-coding, 4% lncRNA, 1% miscRNA, 5% pseudogene	Antigen processing and presentation of exogenous peptide antigen via MHC class II (FDR = 1.26 x 10^{-5};	Integral component of lumenal side of endoplasmic reticulum membrane (FDR = 9.01 x 10^{-9}; FE = 54.08).

				FE = 42.62). Peptide antigen assembly with MHC class II protein complex (FDR = 1.26 x 10^{-5}; FE = 70.46).	Lumenal side of endoplasmic reticulum membrane (FDR = 9.01 x 10^{-9}; FE = 54.08). MHC class II protein complex (FDR = 6.36 x 10^{-8}; FE = 62.26).
9	PAXIP1-AS2	86	90% protein-coding, 5% lncRNA, 2% miscRNA, 3% pseudogene	N/S	Nucleoplasm (FDR = 2.61 x 10^{-8}; FE = 2.33). Nuclear lumen (FDR = 2.22 x 10^{-7}; FE = 2.10). Nuclear part (FDR = 2.22 x 10^{-7}; FE = 2.03).
10	RNU6-840P, RNU6-164P, Y_RNA_ENST00000362962	387	22% protein-coding, 9% lncRNA, 59% miscRNA, 10% pseudogene	N/S	Mitochondrial respiratory chain (FDR = 9.90 x 10^{-5}; FE = 17.06). Inner mitochondrial membrane protein complex (FDR = 9.90 x 10^{-5}; FE = 11.92).
11	RNU6-936P	428	15% protein-coding, 4% lncRNA, 79% miscRNA, 2% pseudogene	RNA processing (FDR = 8.34 x 10^{-11}; FE = 5.44).	Spliceosomal snRNP complex (FDR = 1.05 x 10^{-5}; FE = 21.16). Small nuclear ribonucleoprotein complex (FDR = 1.05 x 10^{-5}; FE = 19.70).
12	ZNF271P	146	87% protein-coding, 6% lncRNA, 3% miscRNA, 3% pseudogene	Nucleic acid metabolic process (FDR = 6.02 x 10^{-7}; FE = 1.85).	Nucleus (FDR = 1.15 x 10^{-5}; FE = 1.50). Centrosome (FDR = 9.18 x 10^{-5}; FE = 3.74).

Biologically relevant modules contained at least one of the 110 hypertrophy-related ncRNA genes, <500 co-expressed genes, and had an FDR of $\leq 5.0 \times 10^{-5}$ for at least one biological process and/or cellular component. For brevity, only 3 enriched gene ontology terms per category are shown; for a complete list of all enriched GO terms, please refer to Supplement Data, S10.

SUPPLEMENTAL MATERIALS

Title: Network-based modelling reveals cell-type enriched patterns of non-coding RNA regulation during human skeletal muscle remodelling

Authors: Jonathan C. Mcleod [1], Changhyun Lim[1,2], Tanner Stokes[1], Jalil-Ahmad Sharif [3], Vagif Zeynalli [1], Lucas Wiens [1], Alysha C D'Souza [1], Lauren Colenso-Semple [1], James McKendry [1,4], Robert W. Morton [1], Cameron J. Mitchell [5], Sara Y. Oikawa [1], Claes Wahlestedt [6], J Paul Chapple [3], Chris McGlory [7], James A. Timmons [3,6*] and Stuart M. Phillips [1*]

Short-title: RNA profiling of ncRNA genes in skeletal muscle

One Sentence Summary: We used an optimised transcriptomic strategy to identify a set of ncRNA genes regulated during skeletal muscle hypertrophy in one hundred and forty-four people, with network modelling and spatial imaging providing biological context.

Key words: Transcriptome, Angiogenesis, Spatial, Muscle Growth, Exercise, Single-Cell, Immune Cell

Affiliations:

[1]Department of Kinesiology, McMaster University, Hamilton, Ontario, Canada.

[2] Population Health Sciences Institute, Faculty of Medical Sciences, Newcastle University, Newcastle upon Tyne, UK

[3] Faculty of Medicine and Dentistry, Queen Mary University London, London, UK.

[4] Faculty of Land and Food Systems, Food, Nutrition & Health, University of British Columbia, BC, Canada

[5] School of Kinesiology, University of British Columbia, BC, Canada

[6] University of Miami Miller School of Medicine, Miami, FL, USA

[7] School of Kinesiology and Health Studies, Queens University, Kingston, ON, Canada

* Joint senior authors

Correspondence to: Jonathan C. Mcleod, Jonathan.mcleod@queensu.ca

Table S1. Demographics of the five studies used for establishing ncRNA genes associated with skeletal muscle hypertrophy.

	Morton et al., 2019 [40]	Morton et al., 2016 [39]	Phillips et al., 2017 [41]	Mitchell et al., 2014 [42]	Stokes et al., 2020 [25]
Sample size, n	32	33	47	20	12
Age, years	22 ± 3 (19 – 28)	23 ± 3 (20 – 29)	38 ± 9 (21 – 51)	24 ± 3 (20 – 30)	21 ± 3 (18 – 29)
Gender, M/F	32/0	33/0	18/29	20/0	12/0
Body mass index, kg/m^2	25 ± 6 (18 – 38)	26 ± 9 (41)	32 ± 4 (26 – 43)	24 ± 4 (15 – 32)	24 ± 3 (20 – 31)
Measurement instrument	DXA	DXA	DXA	MRI	DXA
Limbs Involved in Measurement	1	2	1	1	1
Pre-training LLM, kg	10.3 ± 2.1 (7.2 – 14.6)	24.2 ± 3.0 (17.4 – 30.9)	5.8 ± 1.4 (3.2 – 8.6)	-	9.5 ± 1.6 (7.7 – 13.4)
Post-training LLM, kg	10.6 ± 2.1 (7.6 – 15.2)	25.0 ± 3.0 (19.9 – 31.2)	6.0 ± 1.4 (3.5 – 8.7)	-	9.9 ± 1.6 (8.1 – 13.4)
Pre-training QMV, cm^3	-	-	-	1862.0 ± 402.6 (1039.0 – 2822.0)	-
Post-training QMV, cm^3	-	-	-	1985.0 ± 417.6 (1278.0 – 3104.0)	-
dLLM, %	3.2 ± 3.1 (-3.7 – 9.1)	3.0 ± 5.0 (-5.0 – 19.0)	3.1 ± 3.7 (-4.5 – 11.0)	-	5.0 ± 4.3 (-1.2 – 14.0)
dQMV, %	-	-	-	7.1 ± 7.0 (-1.8 – 24.7)	-
R^2 dLLM (kg) vs Pre-training LLM (kg)	0.07	0.01	< 0.01	-	< 0.01
R^2 dQMV (cm^3) vs Pre-training QMV (cm^3)	-	-	-	< 0.01	-
R^2 dLLM (kg) vs Age (years)	0.26	< 0.01	< 0.01	-	0.04
R^2 dQMV (cm^3) vs Age (years)	-	-	-	0.01	-
R^2 dLLM (kg) vs Gender	-	-	0.04	-	-
LMR group, n	20	20	24	14	10
NMLR group, n	10	13	20	5	2

Age, body mass index, Pre-training LLM, Post-training LLM, dLLM, Pre-training QMV, Post-training QMV, and dQMV are displayed as mean ± SD (min - max). Sample size, Gender, LMR group, and NMLR group are displayed as counts. Abbreviations: DXA, dual X-ray absorptiometry; MRI, magnetic resonance imaging; dLLM, delta leg lean mass; QMV, quadriceps muscle volume; LMR, lean mass responders; NMLR, no measurable lean mass response.

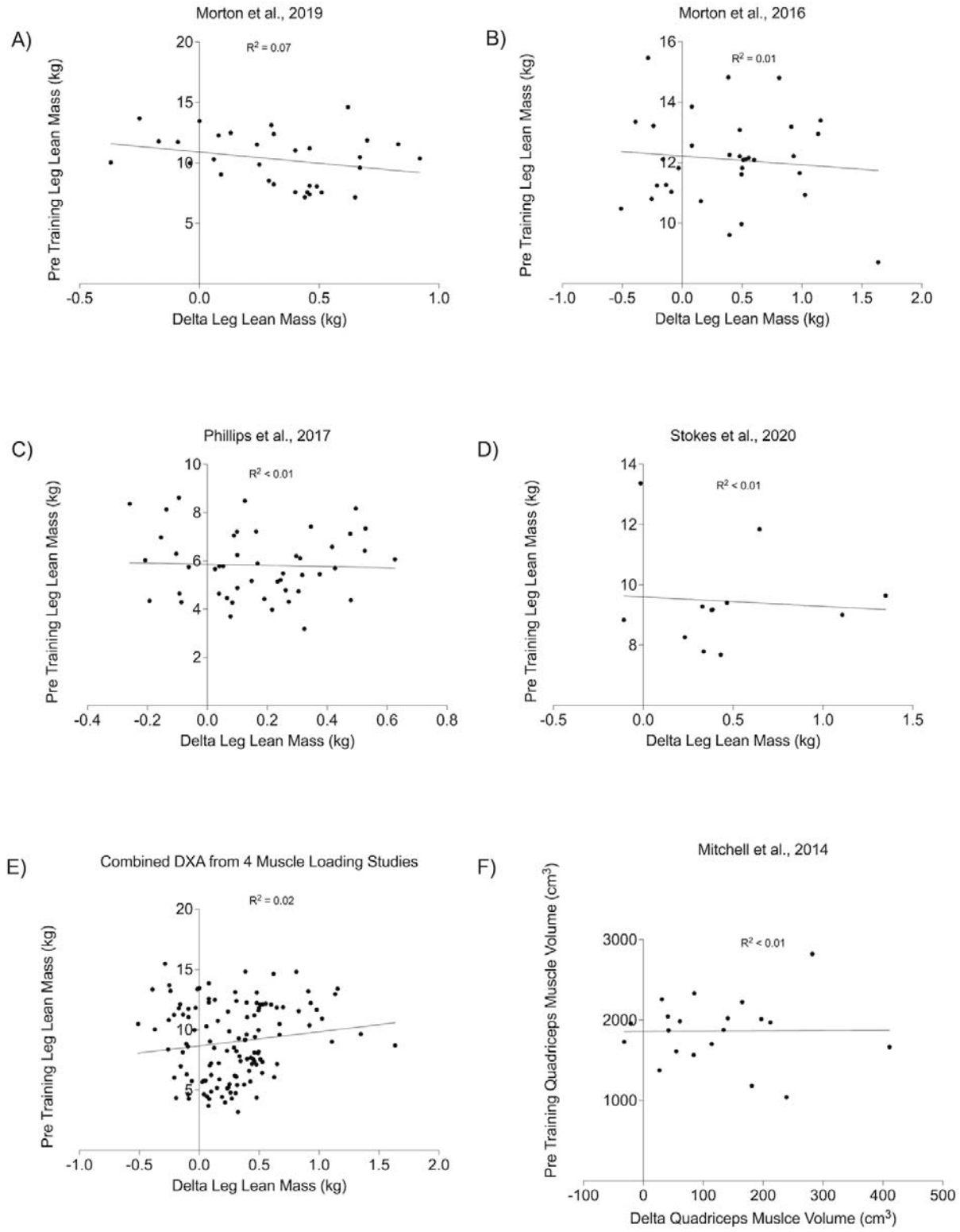

Figure S1. (A-D) Changes in leg lean mass versus pretraining leg lean mass for 4 muscle loading studies, and (E) depicts the aggregated relationship. F) Changes in quadriceps muscle volume vs pre-training quadriceps muscle volume.

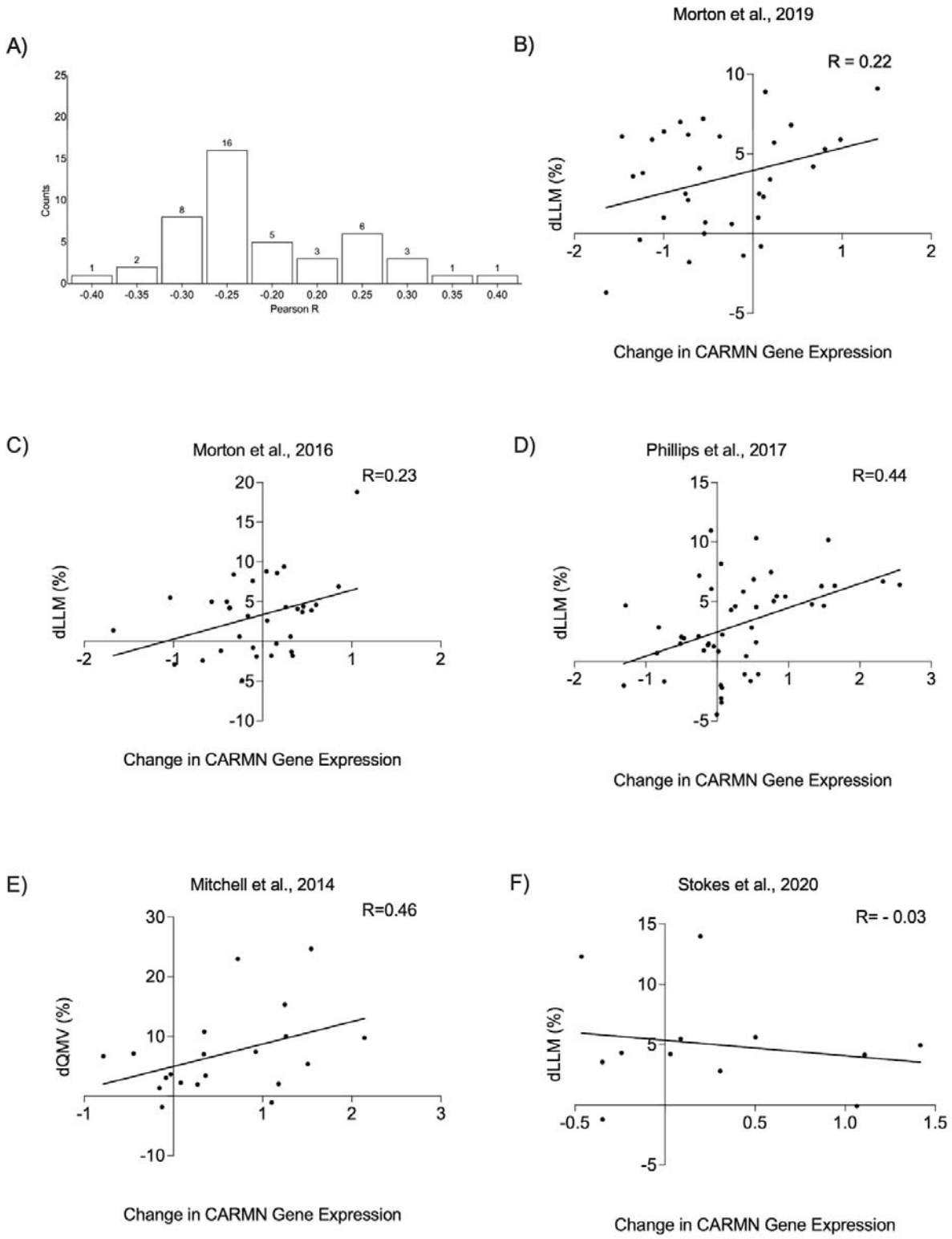

Figure S2. (A) Distribution of Pearson correlation coefficients among the 46 ncRNA genes containing a change in expression that was modestly associated with changes in LLM (dLLM), or changes in Quadriceps muscle volume (dQMV; Supplement Data S5). (B -F) Visual example

from the linear modelling analysis, depicting the relationship between dLLM (or dQMV [E]) and changes in *CARMN* gene expression for each of the 5 individual exercise studies.

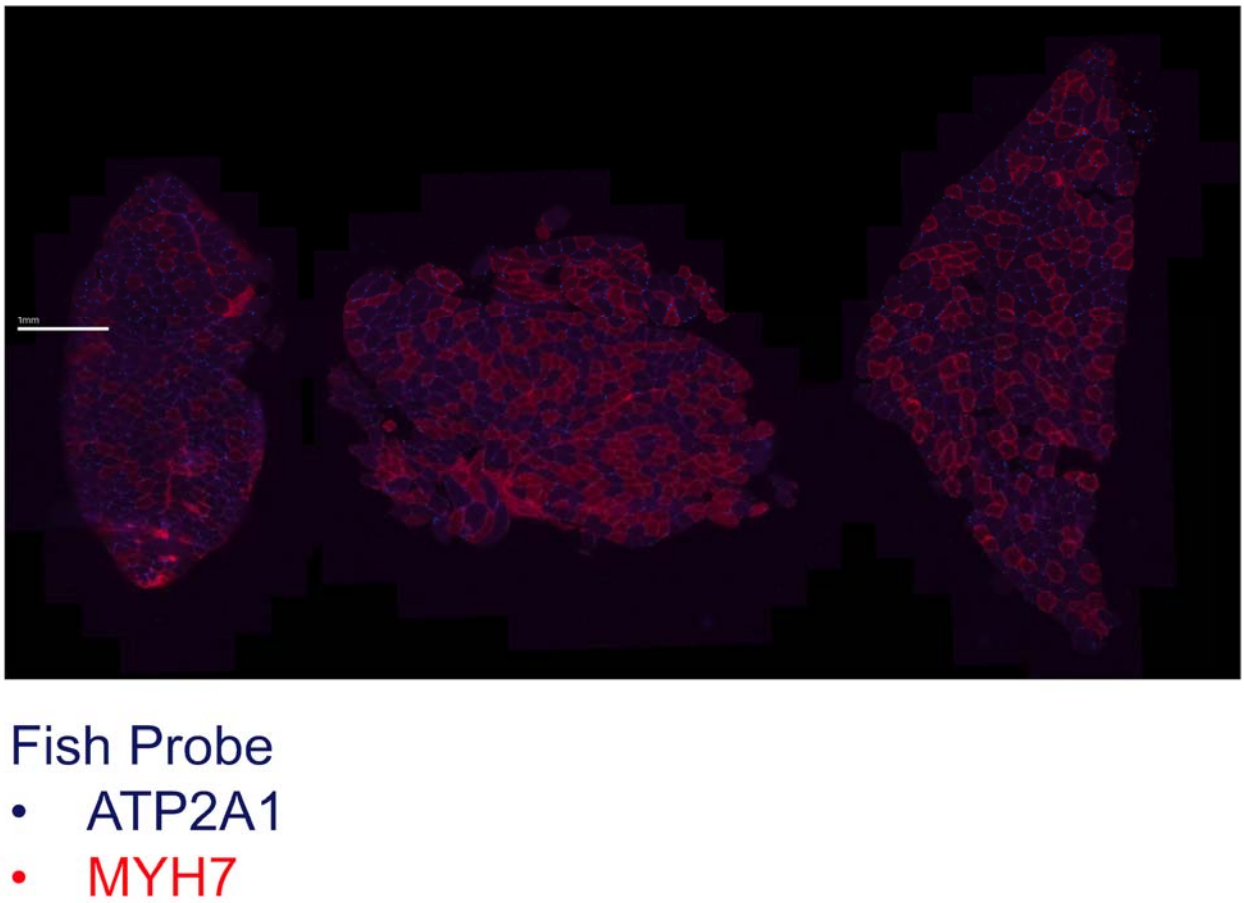

Figure S3. MERSCOPE-MERFISH overview for 3 samples used.

Table S2. Existing biochemical relationship for 110 hypertrophy-related ncRNA genes in skeletal muscle.

ENSG	Gene Symbol	Gene Synonyms	Group Identified In	Pre-existing evidence in skeletal muscle physiology
ENSG00000222041	CYTOR	C2ORF59, LINC00152, MGC4677, NCRNA00152	LMR	Exercise-induced lncRNA that is reduced with ageing. Promotes fast twitch cell fate. Reduces chromatin accessibility and sequesters TEAD1 [26].
ENSG00000268518	ENSG00000268518	MYREM, LNCFAM, LNCFAM71E1-2:2	LMR	Increases during myogenesis and promotes differentiation of myoblasts into myotubes [74]. Increases transcription of myosin binding protein C2 [74].
ENSG00000214548	MEG3	GTL2, LINC00023, NCRNA00023, ONCO-LNCRNA-83	LMR	MEG3 regulates myoblast differentiation [78]. MEG3 knockdown enhances mesenchymal characteristics, impairs myotube formation, and compromises skeletal muscle regeneration [78].
ENSG00000130600	H19	ASM, ASM1, D11S813E, LINC00008, MIR675HG, NCRNA00008	LMR	Predictor VO2max training response [77]. H19-encoded miRNA regulates skeletal muscle growth and translation initiation factors [99]. Maintains slow muscle fibre phenotype, exercise endurance and muscle function in mice [130]. In mice myoblasts, H19 associates with Dystrophin and protects its degradation [100].
ENSG00000241158	ADAMTS9-AS1	NONE	dLLM vs dGE	NONE
ENSG00000262943	ALOX12P2_ENST00000570921	NONE	LMR	NONE
ENSG00000215811	BTNL10P	BTN4, BTNL10, BUTR1	dLLM vs dGE	NONE
ENSG00000254614	CAPN1-AS1	NONE	LMR	NONE
ENSG00000249669	CARMN	CARMEN, MIR143HG	LMR & dLLM vs dGE	NONE
ENSG00000272168	CASC15	LINC00340, LNC-SOX4-1	dLLM vs dGE	NONE
ENSG00000229140	CCDC26	MGC27434, RAM	dLLM vs dGE	NONE
ENSG00000234898	CHEK2P3	NONE	LMR	NONE
ENSG00000229452	CPVL-AS1	NONE	dLLM vs dGE	NONE
ENSG00000226950	DANCR	AGU2, ANCR, KIAA0114, LNCRNA-ANCR, SNHG13	LMR	NONE
ENSG00000233143	DIRC3-AS1	NONE	LMR	NONE
ENSG00000232010	DNMT3L-AS1	NONE	LMR	NONE
ENSG00000223668	EEF1A1P24	NONE	LMR	NONE
ENSG00000149656	ENSG00000149656	NONE	NMLMR	NONE
ENSG00000176349	ENSG00000176349	NONE	dLLM vs dGE	NONE
ENSG00000213963	ENSG00000213963	NONE	NMLMR	NONE
ENSG00000214942	ENSG00000214942	NONE	LMR	NONE
ENSG00000228778	ENSG00000228778	NONE	dLLM vs dGE	NONE
ENSG00000229425	ENSG00000229425	NONE	LMR	NONE
ENSG00000230947	ENSG00000230947	NONE	dLLM vs dGE	NONE
ENSG00000231927	ENSG00000231927	NONE	dLLM vs dGE	NONE
ENSG00000234139	ENSG00000234139	NONE	dLLM vs dGE	NONE
ENSG00000234677	ENSG00000234677	NONE	dLLM vs dGE	NONE
ENSG00000236234	ENSG00000236234	NONE	dLLM vs dGE	NONE
ENSG00000236601	ENSG00000236601	NONE	LMR	NONE

ENSG00000237035	ENSG00000237035	NONE	dLLM vs dGE	NONE
ENSG00000238142	ENSG00000238142	NONE	NMLMR	NONE
ENSG00000249021	ENSG00000249021	NONE	LMR	NONE
ENSG00000250978	ENSG00000250978	NONE	LMR	NONE
ENSG00000251511	ENSG00000251511	NONE	dLLM vs dGE	NONE
ENSG00000252230	ENSG00000252230	NONE	NMLMR	NONE
ENSG00000253553	ENSG00000253553	NONE	dLLM vs dGE	NONE
ENSG00000254409	ENSG00000254409	NONE	NMLMR	NONE
ENSG00000254641	ENSG00000254641	NONE	LMR	NONE
ENSG00000254975	ENSG00000254975	NONE	dLLM vs dGE	NONE
ENSG00000255313	ENSG00000255313	NONE	dLLM vs dGE	NONE
ENSG00000255689	ENSG00000255689	NONE	LMR	NONE
ENSG00000258649	ENSG00000258649	NONE	dLLM vs dGE	NONE
ENSG00000258760	ENSG00000258760	NONE	NMLMR	NONE
ENSG00000260971	ENSG00000260971	NONE	NMLMR	NONE
ENSG00000261327	ENSG00000261327	NONE	dLLM vs dGE	NONE
ENSG00000263618	ENSG00000263618	NONE	LMR	NONE
ENSG00000267784	ENSG00000267784	NONE	LMR	NONE
ENSG00000273674	ENSG00000273674	NONE	dLLM vs dGE	NONE
ENSG00000279482	ENSG00000279482	NONE	LMR	NONE
ENSG00000285945	ENSG00000285945	NONE	LMR	NONE
ENSG00000286829	ENSG00000286829	NONE	LMR	NONE
ENSG00000288253	ENSG00000288253	NONE	dLLM vs dGE	NONE
ENSG00000289228	ENSG00000289228	NONE	LMR	NONE
ENSG00000290482	ENSG00000290482	NONE	dLLM vs dGE	NONE
ENSG00000291041	ENSG00000291041	NONE	LMR	NONE
ENSG00000273100	ENST00000610240	NONE	LMR	NONE
ENSG00000275563	ENST00000613990	NONE	LMR	NONE
ENSG00000260528	FAM157C	NONE	NMLMR	NONE
ENSG00000251402	FAM90A25P	NONE	LMR	NONE
ENSG00000256943	GALNT9-AS1	NONE	dLLM vs dGE	NONE
ENSG00000224934	GOT1-DT	NONE	LMR	NONE
ENSG00000179362	HMGN2P46	C15ORF21, D-PCA-2, FLJ39426	dLLM vs dGE	NONE
ENSG00000224699	LAMTOR5-AS1	NONE	dLLM vs dGE	NONE
ENSG00000230710	LINC00332	NCRNA00332	LMR	NONE
ENSG00000226519	LINC00390	TCONS_00021641	LMR	NONE
ENSG00000236678	LINC00347	NONE	LMR	NONE
ENSG00000225179	LINC00457	NONE	dLLM vs dGE	NONE
ENSG00000233723	LINC01122	AC007092.1, FLJ30838	dLLM vs dGE	NONE

ENSG00000233985	LINC01681	NONE	dLLM vs dGE	NONE
ENSG00000226983	LINC01692	NONE	dLLM vs dGE	NONE
ENSG00000237166	LINC01792	NONE	dLLM vs dGE	NONE
ENSG00000267057	LINC01905	NONE	LMR	NONE
ENSG00000204650	LINC02210	C17ORF69, C17orf69, CRHR1-IT1, FLJ25168	NMLMR	NONE
ENSG00000229536	LINC02572	AC079776.2	NMLMR	NONE
ENSG00000233593	LINC02609	NONE	dLLM vs dGE	NONE
ENSG00000234222	LIX1L-AS1	NONE	LMR	NONE
ENSG00000267023	LRRC37A16P	NONE	LMR	NONE
ENSG00000254349	MIR2052HG	NONE	NMLMR	NONE
ENSG00000172965	MIR4435-2HG	AGD2, AK001796, LINC00978, LNCRNA-AWPPH, MIR4435-1HG, MORRBID	LMR	NONE
ENSG00000197182	MIRLET7BHG	LINC-PPARA	dLLM vs dGE	NONE
ENSG00000238151	MLLT10P1	BA348I14.3, MLLT10L	LMR	NONE
ENSG00000242086	MUC20-OT1	NONE	LMR	NONE
ENSG00000214106	PAXIP1-AS2	PAXIP1OS	dLLM vs dGE	NONE
ENSG00000229941	PDE11A-AS1	NONE	dLLM vs dGE	NONE
ENSG00000249996	PPIC-AS1	NONE	dLLM vs dGE	NONE
ENSG00000226833	PPP1CB-DT	NONE	NMLMR	NONE
ENSG00000214182	PTMAP5	NONE	LMR	NONE
ENSG00000201875	RN7SKP178	NONE	LMR	NONE
ENSG00000275776	RN7SL185P	NONE	LMR	NONE
ENSG00000239468	RN7SL569P	NONE	dLLM vs dGE	NONE
ENSG00000239899	RN7SL674P	NONE	NMLMR	NONE
ENSG00000252957	RNA5SP402	NONE	dLLM vs dGE	NONE
ENSG00000201474	RNU6-164P	NONE	LMR	NONE
ENSG00000253084	RNU6-840P	NONE	LMR	NONE
ENSG00000199260	RNU6-874P	NONE	dLLM vs dGE	NONE
ENSG00000206732	RNU6-936P	NONE	dLLM vs dGE	NONE
ENSG00000230438	SERPINB9P1	MGC39372	LMR	NONE
ENSG00000234899	SOX9-AS1	NONE	LMR	NONE
ENSG00000187653	TMSB4XP8	TMSL3	LMR	NONE
ENSG00000232600	TONSL-AS1	NONE	dLLM vs dGE	NONE
ENSG00000237298	TTN-AS1	NONE	LMR	NONE
ENSG00000273249	WDR5-DT	NONE	NMLMR	NONE
ENSG00000199332	Y_RNA_ENST00000362462	NONE	NMLMR	NONE
ENSG00000199832	Y_RNA_ENST00000362962	NONE	LMR	NONE
ENSG00000212556	Y_RNA_ENST00000391254	NONE	dLLM vs dGE	NONE

ENSG00000252759	Y_RNA_ENST00000516950	NONE	dLLM vs dGE	NONE
ENSG00000252915	Y_RNA_ENST00000517106	NONE	dLLM vs dGE	NONE
ENSG00000250802	ZBED3-AS1	LNC13728	dLLM vs dGE	NONE
ENSG00000263072	ZNF213-AS1	NONE	dLLM vs dGE	NONE
ENSG00000257267	ZNF271P	HZF7, ZNF271, ZNFEB	LMR	NONE

A systematic PUBMED search was carried out on March 19th, 2024, using the gene symbol (and using any related gene synonyms found on Ensembl (https://useast.ensembl.org/index.html), and the following terms: “skeletal muscle” AND “myotubes” AND “myocytes”. Relevant articles were examined to determine a clear role in skeletal muscle physiology.

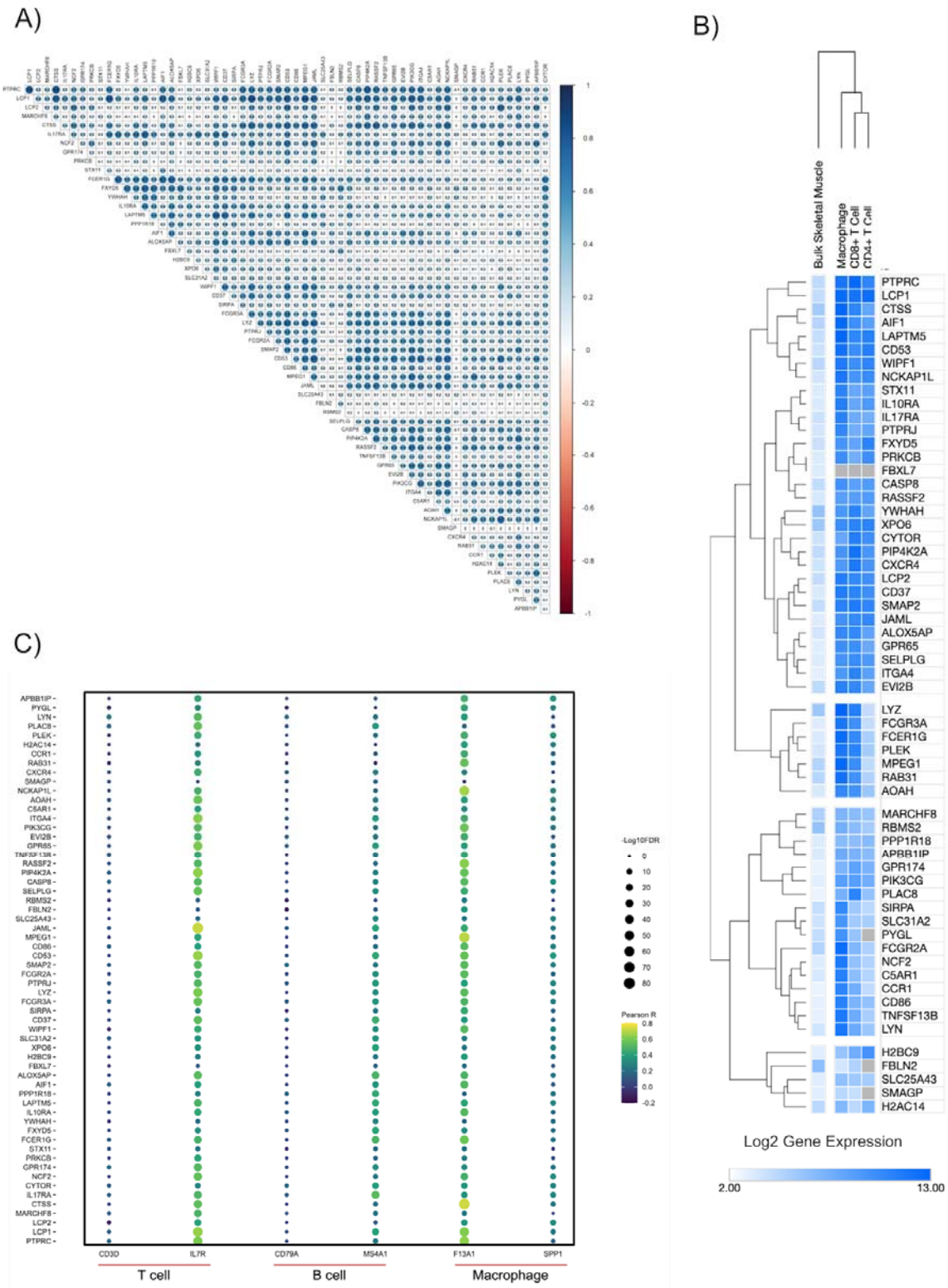

Figure S4. A) Pearson correlation matrix of all 60 genes co-expressed in network 1. Majority of the genes are positively correlated with each other in this network. B) the heatmap uses the log2 gene expression in skeletal muscle (n=437) and plots the 60 genes co-expressed in network 1

along with marker genes from three mononuclear cells of the immune system (macrophages, CD4 T-cells, and CD8 T-cells). The plot was created using Morpheus (https://clue.io/Morpheus), and genes and tissue types were hierarchically clustered using Euclidean distance (linkage method: complete). C) Dot plot depicting the association between the expression of network 1 genes, and gene markers for T-cells, B-cells and macrophages, in human skeletal muscle transcriptomic data (n=437). The colouring of the dot corresponds to the Pearson correlation coefficient, and the size of the dot is proportional to the $-Log^{10}$ FDR.

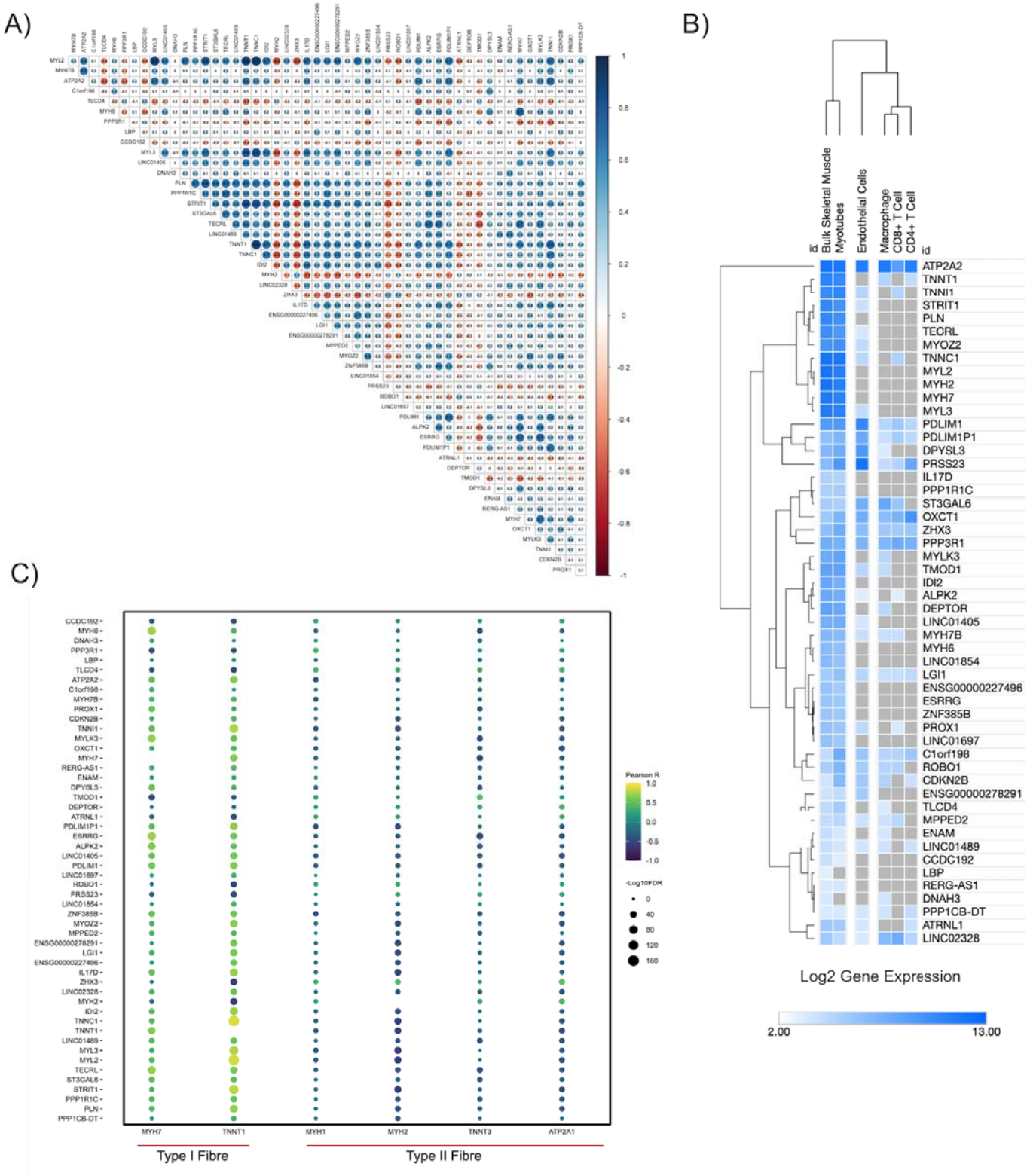

Figure S5. A) Pearson correlation matrix of all 52 genes co-expressed in network 2. Majority of the genes are positively correlated with each other in this network. b) the heatmap uses the log2

gene expression in skeletal muscle (n=437) and plots the 52 genes co-expressed in network 2 along with marker genes from bulk skeletal muscle, myotubes, endothelial cells, and three mononuclear cells of the immune system (macrophages, CD4 T-cells, and CD8 T-cells). The plot was created using Morpheus (https://clue.io/Morpheus), and genes and tissue types were hierarchically clustered using Euclidean distance (linkage method: complete). C) Dot plot depicting the association between the expression of network 2 genes, and gene markers for type I and type II fiber in human skeletal muscle transcriptomic data (n=437). The colouring of the dot corresponds to the Pearson correlation coefficient, and the size of the dot is proportional to the $-\mathrm{Log}^{10}$ FDR.

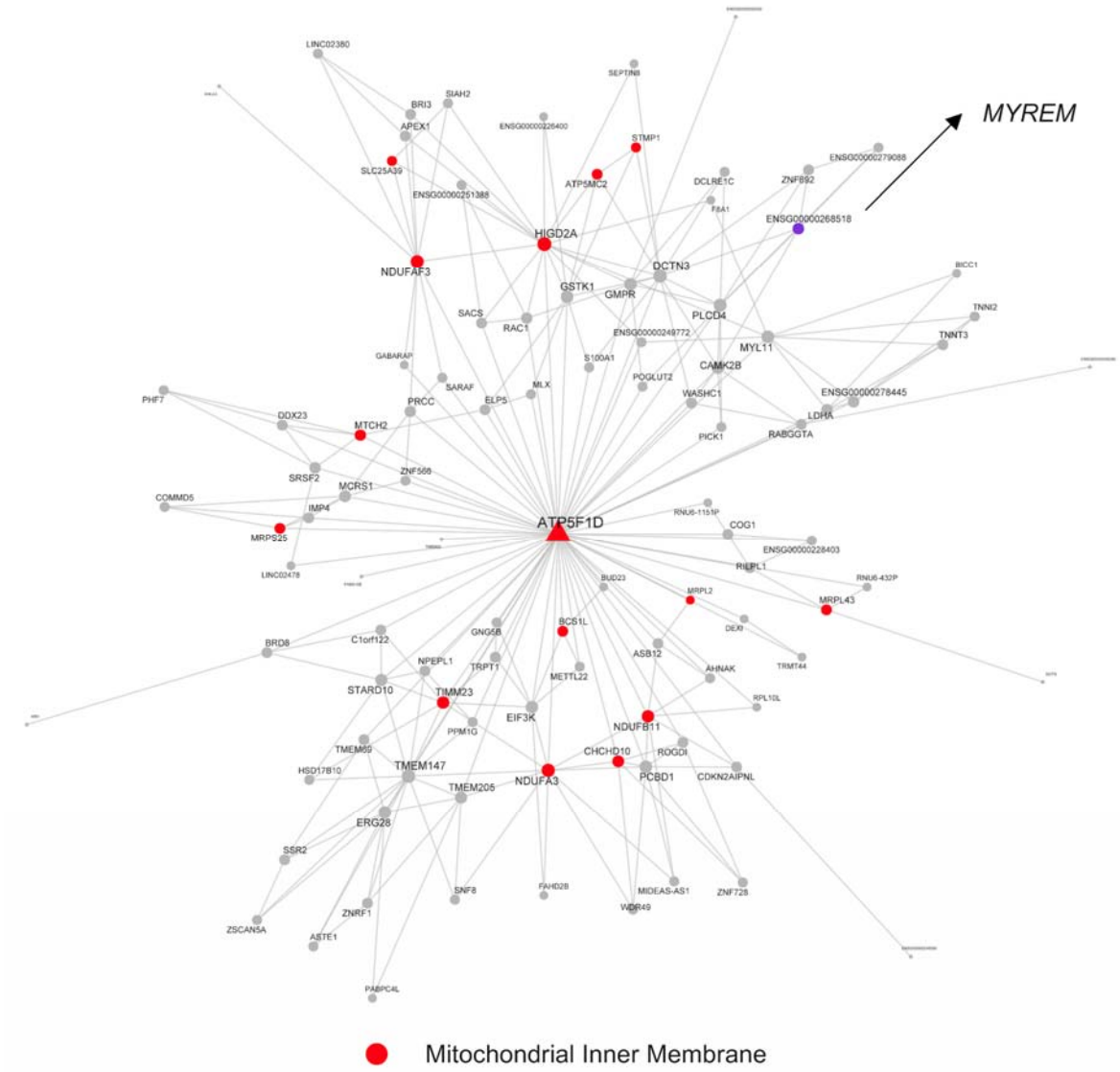

Figure S6. A mitochondrial-related gene co-expression network (network 4; Table 1) that contains the hypertrophy-related ncRNA gene, *MYREM* (purple).

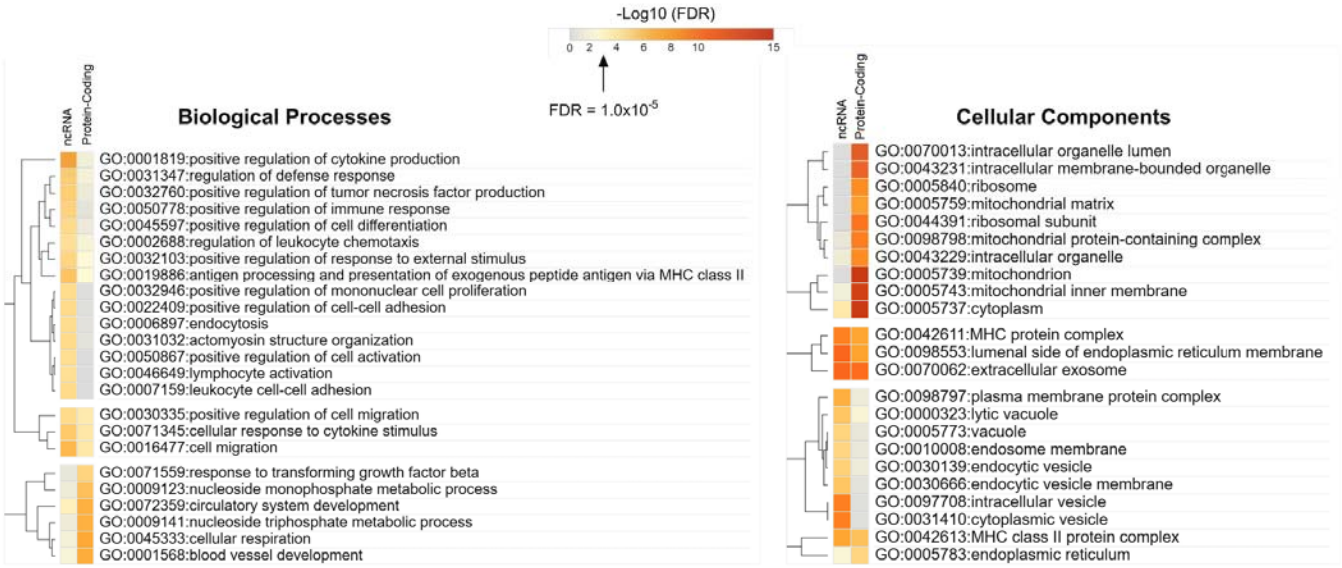

Figure S7. Similarities and differences in significant GO terms (biological processes and cellular components) across ncRNA MEGENA networks and our previously reported growth-regulated protein-coding MEGENA networks [25]. The heatplot was created using Morpheus (https://clue.io/Morpheus), and genes and tissue types were hierarchically clustered using Euclidean distance (linkage method: complete).